

Electronic Supplemental Information for

Photochemistry and *in vitro* anticancer activity of Pt(IV)Re(I) conjugates

Zhouyang Huang,^a A. Paden King,^a James Lovett,^b Barry Lai,^c Joshua J. Woods,^{a,d} Hugh H. Harris,^b and Justin J. Wilson*^a

^aDepartment of Chemistry and Chemical Biology, Cornell University, Ithaca, NY 14853, USA.

^bDepartment of Chemistry, The University of Adelaide, South Australia 5005, Australia.

^cAdvanced Photon Source, X-ray Science Division, Argonne National Laboratory, Argonne, IL 60439, USA.

^dRobert F. Smith School for Chemical and Biomolecular Engineering, Cornell University, Ithaca, NY 14853, USA.

*Email: jjw275@cornell.edu

Table of Contents

General

Synthesis and Characterization

Stability and Decomposition Studies

Photophysical and Photochemical Studies

Electrochemical Studies

Computational Studies

Cellular Studies

XRF Imaging Studies

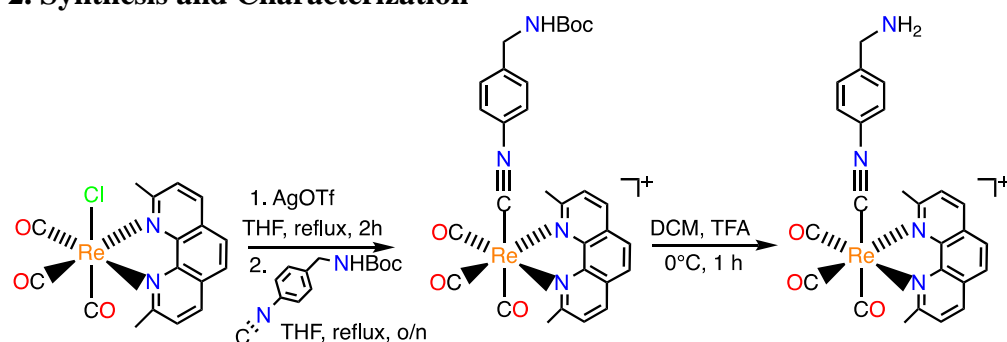
References

1. General

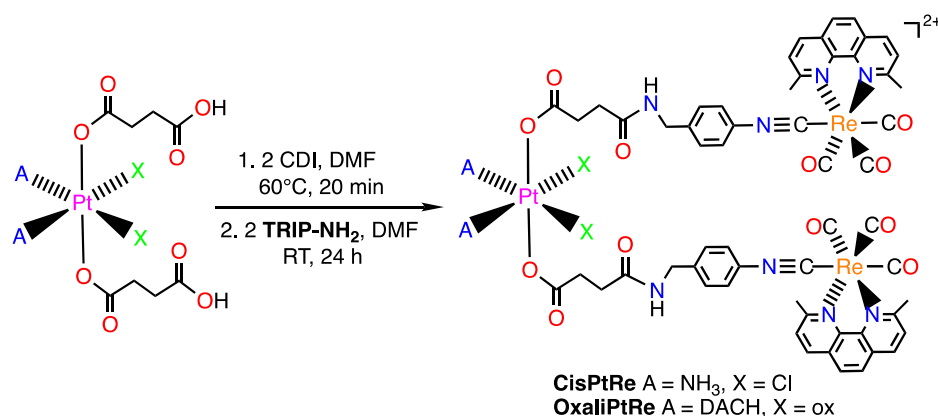
Materials and Reagents. All reagents were purchased from commercial vendors. All solvents were of ACS grade or higher. Dry solvents were stored over 4 Å molecular sieves. $[\text{Re}(\text{CO})_3(\text{dmphen})\text{Cl}]$,¹ *cis,cis,trans*- $[\text{Pt}(\text{NH}_3)_2\text{Cl}_2(\text{suc})_2]$,² *trans*- $[\text{Pt}(\text{DACH})(\text{ox})(\text{suc})_2]$ ² (dmphen = 2,9-dimethyl-1,10-phenanthroline, suc = succinate, DACH = 1*R*,2*R*-diaminocyclohexane, ox = oxalate), and 4-(*N*-Boc-aminomethyl)aniline³ were synthesized as previously described. Unless otherwise noted, no specific precautions were taken to exclude air or water from reactions.

Physical Measurements. NMR samples were prepared in DMSO-*d*₆ and analyzed on a 500 MHz Bruker AV 3HD spectrometer equipped with a broadband Prodigy cryoprobe. ¹H NMR chemical shifts were referenced internally to tetramethylsilane ($\delta = 0$ ppm). ¹⁹⁵Pt chemical shifts were referenced to Na₂[PtCl₆] ($\delta = 0$ ppm) with an external standard of K₂[PtCl₄] in D₂O ($\delta = -1628$ ppm). ¹⁹F chemical shifts were referenced to CFCl₃ ($\delta = 0$ ppm) with an external standard of KPF₆ in D₂O ($\delta = -72$ ppm). Fourier transform infrared spectra were acquired with a Thermo Nicolet Avatar 370 DTGS FTIR spectrometer using samples prepared as KBr pellets. High-resolution electrospray mass spectrometry (HR-ESI-MS) measurements were obtained on an Exactive Orbitrap mass spectrometer in positive ion mode (ThermoFisher Scientific, Waltham, MA). Elemental analysis (CHN) was performed by Atlantic Microlab Inc. (Norcross, GA, USA). High-performance liquid chromatography (HPLC) was carried out on a system consisted of a CBM-20A communications bus module, an LC-20AP (preparative) or LC-20AT (analytical) pump, and an SPD-20AV UV-Vis detector monitoring at 270 nm (Shimadzu, Japan). Semipreparative HPLC purification used an Epic Polar preparative column, 120 Å, 10 μm , 25 cm \times 20 mm (ES Industries, West Berlin, NJ) at a flow rate of 14 mL/min. Analytical HPLC was carried out using an Ultra Aqueous C18 column, 100 Å, 5 μm , 250 mm \times 4.6 mm (Restek, Bellefonte, PA) at a flow rate of 1.0 mL/min. All HPLC methods employed use a binary mobile phase (H₂O and MeOH) containing 0.1% trifluoroacetic acid (TFA). For preparative HPLC, gradients were described in the synthesis section below. For analytical HPLC, the following gradient was used: 0–5 min, 10% MeOH; 5–25 min, 10–100% MeOH; 25–30 min, 100% MeOH. UV-vis spectra were acquired using a Shimadzu UV-1900 spectrophotometer (Shimadzu, Kyoto, Japan) fitted with a temperature-controlled circulating water bath. Emission spectra were acquired using a Varian Eclipse Fluorometer. For analytical photochemical measurements, irradiation was performed using a Newport mercury/xenon arc lamp. The light output was modulated using a combination of a Newport heat-absorbing glass filter (50.8 \times 50.8 mm) with infrared cutoff (Schott KG5 filter glass), a Newport mercury line bandpass filter (25.4 mm, center wavelength 365.0 \pm 2 nm), and a Newport visible absorbing filter (50.8 \times 50.8 mm, center wavelength 340 nm) made of dark optical glass to isolate monochromatic 365 nm light.

2. Synthesis and Characterization



Scheme S1 Synthetic scheme for the preparation of **TRIP-NH₂**.



Scheme S2 Synthetic scheme for the preparation of **CisPtRe** and **OxaliPtRe**.

Synthesis of 4-(*N*-Boc-aminomethyl)phenylisonitrile. This compound was prepared using slight modifications to the Hofmann isonitrile synthesis.⁴ To a stirring solution of 4-(*N*-Boc-aminomethyl)aniline (3.64 g, 16.4 mmol) in DCM (25 mL) were added [NEt₃Bn]Cl (800 mg, 3.5 mmol) and CHCl₃ (1.3 mL, 16.2 mmol). This mixture was then added dropwise to a stirring aqueous KOH solution (23 mL, 1 g/mL) cooled to 0 °C. The resulting biphasic mixture was stirred for 5 h as the solution was allowed to warm to room temperature. DCM was then removed under reduced pressure, and Et₂O (100 mL) was added to the remaining aqueous mixture. The organic layer was extracted with saturated aqueous NaHCO₃ (2 × 75 mL) and then with 0.1 M HCl (2 × 75 mL). The Et₂O fraction was dried over Na₂SO₄, and the solvent was evaporated under reduced pressure to yield a red brown powder. Yield: 1.36 g (5.86 mmol, 36%). The material was used in the next step without further purification. The characterization of this product has been previously reported in the literature.⁵

Synthesis of TRIP-NH₂. To a stirring solution of [Re(CO)₃(dmphen)Cl] (325 mg, 0.63 mmol) in dry THF (25 mL) under an atmosphere of N₂, AgOTf (162 mg, 0.63 mmol) was added, and the resulting mixture was heated at reflux for 3 h in the dark. The white precipitate AgCl was removed via vacuum filtration, and 4-(*N*-Boc-aminomethyl)phenylisonitrile (456 mg, 1.97 mmol) was added to the yellow filtrate. After heating this solution at reflux for 15 h in the dark under N₂, the THF was removed under reduced pressure, and the remaining residue was dissolved in 5 mL of DCM. To this DCM solution, 5 mL of TFA was added dropwise, and the mixture was stirred at 0 °C for 1 h. The solvents were then removed under reduced pressure, yielding an orange oil that was dissolved in 10 mL of 50:50 MeOH:H₂O (containing 0.1% TFA), filtered, and subjected to purification using preparatory RP-HPLC with a MeOH/H₂O (containing 0.1% TFA) gradient: 0–5 min, 50% MeOH; 5–30 min, 50–100% MeOH. The

fractions containing the product were dried by rotary evaporation and lyophilization to yield a yellow powder. Yield: 387 mg (0.46 mmol, 73%). ^1H NMR (500 MHz, DMSO- d_6): δ 8.88 (d, $J = 8.4$ Hz, 2H), 8.25 (s, 2H), 8.20 (d, $J = 8.4$ Hz, 2H), 8.15 (br s, 2H), 7.45 (d, $J = 8.7$ Hz, 2H), 7.41 (d, $J = 8.7$ Hz, 2H), 4.02 (q, $J = 5.8$ Hz, 2H), 3.31 (s, 6H). ^{19}F NMR (470 MHz, DMSO- d_6): δ -73.9. IR (KBr, cm^{-1}): 2180 m, 2038 s, 1967 s, 1933 s. ESI-MS (positive ion mode): m/z 611.1077 ($[\text{M}]^+$, calcd 611.1088). Anal. Calcd for $\text{C}_{25}\text{H}_{21}\text{N}_4\text{O}_3\text{Re}\cdot 2\text{TFA}\cdot 3\text{H}_2\text{O}$: C, 39.06; H, 3.05; N, 6.28. Found: C, 39.05; H, 2.57; N, 6.11.

Synthesis of CisPtRe. A solution of *cis,cis,trans*-[Pt(NH₃)₂Cl₂(suc)₂] (64 mg, 0.12 mmol) in dry DMF (4.5 mL) was added to 1,1'-carbonyldiimidazole (CDI; 38 mg, 0.23 mmol) while stirring. The mixture was heated at 60 °C for 20 min. After the solution was allowed to cool to room temperature, **TRIP-NH₂** (200 mg, 0.24 mmol) in dry DMF (4.5 mL) was added, and the mixture was stirred for 24 h at room temperature in the dark. The DMF was removed under reduced pressure, and the remaining yellow oil was dissolved in 6 mL of 60:40 MeOH:H₂O (containing 0.1% TFA), filtered, and subjected to purification using preparatory RP-HPLC with a MeOH/H₂O (containing 0.1% TFA) gradient: 0–5 min, 60% MeOH; 5–25 min, 60–75% MeOH; 25–30 min, 75–100% MeOH. The fractions containing the product were dried by rotary evaporation and lyophilization to yield a yellow powder. Yield: 52 mg (0.027 mmol, 23%). ^1H NMR (500 MHz, DMSO- d_6): δ 8.88 (d, $J = 8.4$ Hz, 4H), 8.38 (t, $J = 6.1$ Hz, 2H), 8.25 (s, 4H), 8.19 (d, $J = 8.4$ Hz, 4H), 7.24 (s, 8H), 6.48 (br s, 6H), 4.21 (d, $J = 6.0$ Hz, 4H), 3.30 (s, 12H), 2.46 (t, $J = 7.4$ Hz, 4H), 2.31 (t, $J = 7.4$ Hz, 4H). ^{19}F NMR (470 MHz, DMSO- d_6): δ -73.5. $^{195}\text{Pt}\{^1\text{H}\}$ NMR (108 MHz, DMSO- d_6): δ 1221. IR (KBr, cm^{-1}): 2179 m, 2036 s, 1964 s, 1932 s. ESI-MS (positive ion mode): m/z 859.5916 ($[\text{M}]^{2+}$, calcd 859.5940). Anal. Calcd for $\text{C}_{58}\text{H}_{52}\text{Cl}_2\text{N}_{10}\text{O}_{12}\text{PtRe}_2\cdot 2\text{TFA}\cdot 5\text{H}_2\text{O}$: C, 36.58; H, 3.07; N, 6.88. Found: C, 36.69; H, 2.80; N, 6.71.

Synthesis of OxaliPtRe. A solution of *trans*-[Pt(DACH)(ox)(suc)₂] (70 mg, 0.11 mmol) in dry DMF (4.5 mL) was added to CDI (37 mg, 0.23 mmol) while stirring. The mixture was heated at 60 °C for 20 min. After allowing the solution to cool to room temperature, **TRIP-NH₂** (190 mg, 0.23 mmol) in dry DMF (4.5 mL) was added, and the mixture was stirred for 24 h at room temperature in the dark. The DMF was removed under reduced pressure, and the remaining yellow oil was dissolved in 6 mL of 60:40 MeOH:H₂O (containing 0.1% TFA), filtered, and subjected to purification with preparatory RP-HPLC with a MeOH/H₂O (containing 0.1% TFA) gradient: 0–5 min, 60% MeOH; 5–25 min, 60–75% MeOH; 25–30 min, 75–100% MeOH. The fractions containing the product were dried by rotary evaporation and lyophilization to yield a yellow powder. Yield: 120 mg (0.059 mmol, 53%). ^1H NMR (500 MHz, DMSO- d_6): δ 8.86 (d, $J = 8.4$ Hz, 4H), 8.40 (t, $J = 6.0$ Hz, 2H), 8.27 (m, 2H), 8.24 (s, 4H), 8.18 (d, $J = 8.4$ Hz, 4H), 8.03 (m, 2H), 7.25 (d, $J = 8.5$ Hz, 4H), 7.23 (d, $J = 8.5$ Hz, 4H), 4.19 (d, $J = 6.0$ Hz, 4H), 3.29 (s, 12H), 2.53 (m, 6H), 2.30 (m, 4H), 1.94 (m, 2H), 1.26 (m, 4H), 0.97 (m, 2H). ^{19}F NMR (470 MHz, DMSO- d_6): δ -73.6. $^{195}\text{Pt}\{^1\text{H}\}$ NMR (108 MHz, DMSO- d_6): δ 1620. IR (KBr, cm^{-1}): 2178 m, 2038 s, 1966 s, 1933 s. ESI-MS (positive ion mode): m/z 908.6409 ($[\text{M}]^{2+}$, calcd 908.6475). Anal. Calcd for $\text{C}_{66}\text{H}_{60}\text{N}_{10}\text{O}_{16}\text{PtRe}_2\cdot 2\text{TFA}\cdot 6\text{H}_2\text{O}$: C, 39.09; H, 3.37; N, 6.51. Found: C, 38.72; H, 2.79; N, 6.26.

Synthesis of TRIP-suc. A solution of **TRIP-NH₂** (85 mg, 0.10 mmol) in dry MeCN (2 mL) was added to succinic anhydride (22 mg, 0.22 mmol) while stirring. The mixture was heated at 60 °C for 2 h in the dark, and then the solvent was removed under reduced pressure. The remaining yellow oil was dissolved in 2 mL of 50:50 MeOH:H₂O (containing 0.1% TFA), filtered, and subjected to purification by preparatory RP-HPLC with a MeOH/H₂O (containing

0.1% TFA) gradient: 0–5 min, 50% MeOH; 5–45 min, 50–100% MeOH. The fractions containing the product were dried by rotary evaporation and lyophilization to yield a yellow powder. Yield: 43 mg (0.052 mmol, 52%). ^1H NMR (500 MHz, $\text{DMSO-}d_6$): δ 12.04 (br s, 1H), 8.87 (d, $J = 8.4$ Hz, 2H), 8.38 (t, $J = 6.0$ Hz, 1H), 8.25 (s, 2H), 8.19 (d, $J = 8.4$ Hz, 2H), 7.23 (s, 4H), 4.20 (d, $J = 6.0$ Hz, 2H), 3.30 (s, 6H), 2.40 (t, $J = 6.3$ Hz, 2H), 2.33 (t, $J = 6.6$ Hz, 2H). ^{19}F NMR (470 MHz, $\text{DMSO-}d_6$): δ -73.5. IR (KBr, cm^{-1}): 2181 m, 2035 s, 1960 s, 1931 s. ESI-MS (positive ion mode): m/z 711.1233 ($[\text{M}]^+$, calcd 711.1249). Anal. Calcd for $\text{C}_{29}\text{H}_{24}\text{N}_4\text{O}_6\text{Re}\cdot\text{TFA}\cdot 2\text{H}_2\text{O}$: C, 43.31; H, 3.28; N, 6.52. Found: C, 43.52; H, 2.92; N, 6.55.

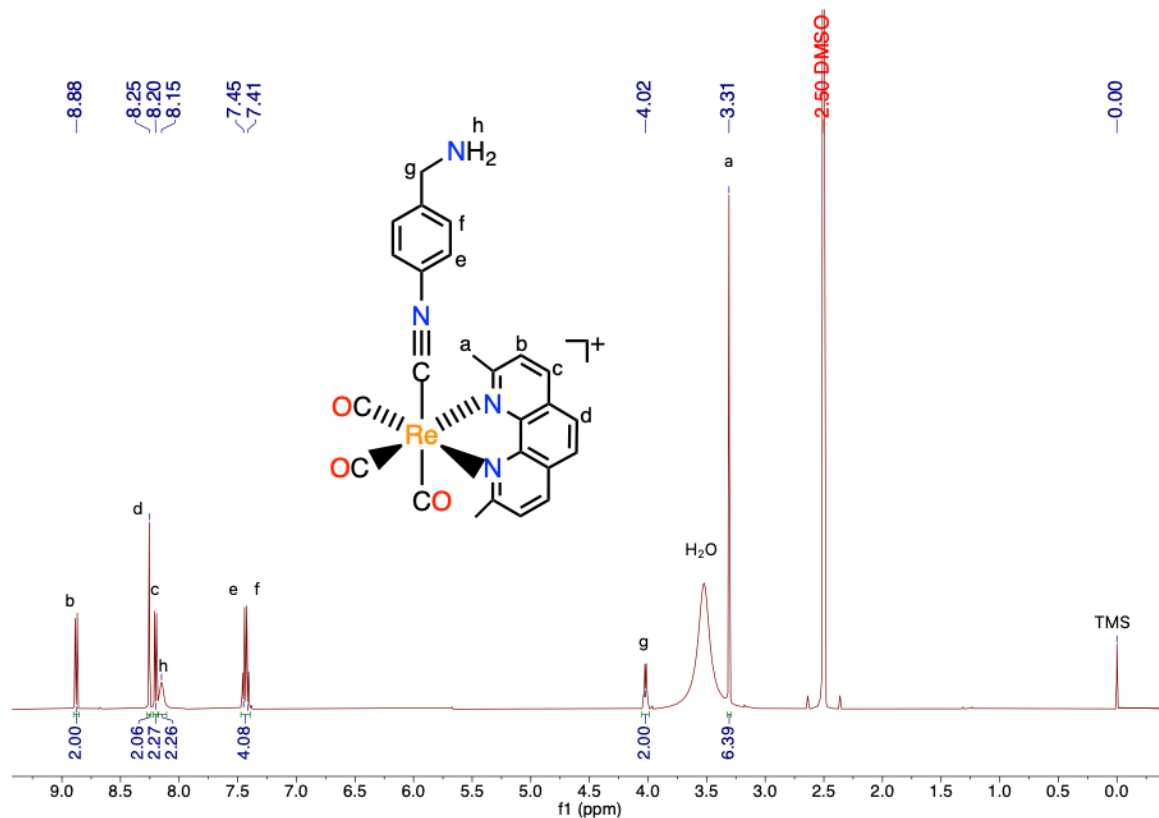


Fig. S1 ^1H NMR spectrum of TRIP-NH₂ in DMSO-*d*₆ (500 MHz, 25 °C).

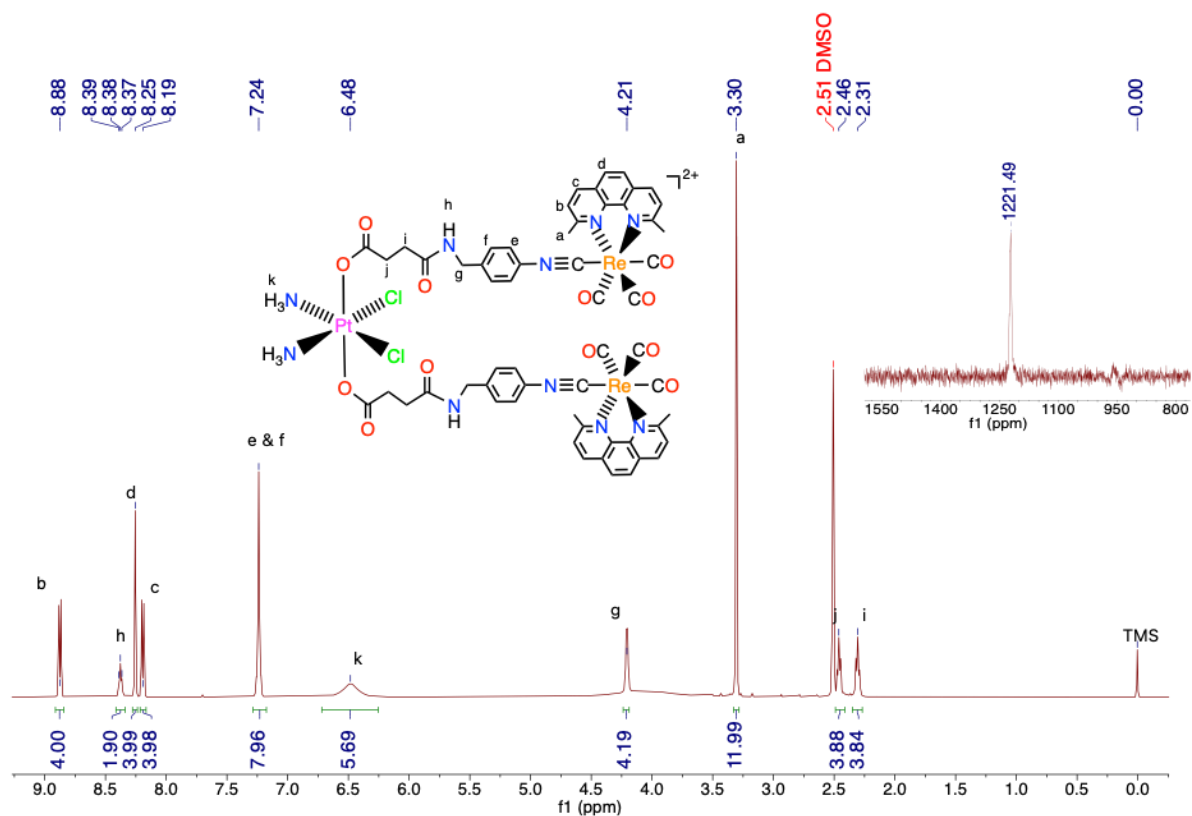


Fig. S2 ^1H NMR spectrum of **CisPtRe** in DMSO- d_6 (500 MHz, 25 °C). Inset: ^{195}Pt NMR spectrum of **CisPtRe** in DMSO- d_6 (108 MHz, 25 °C).

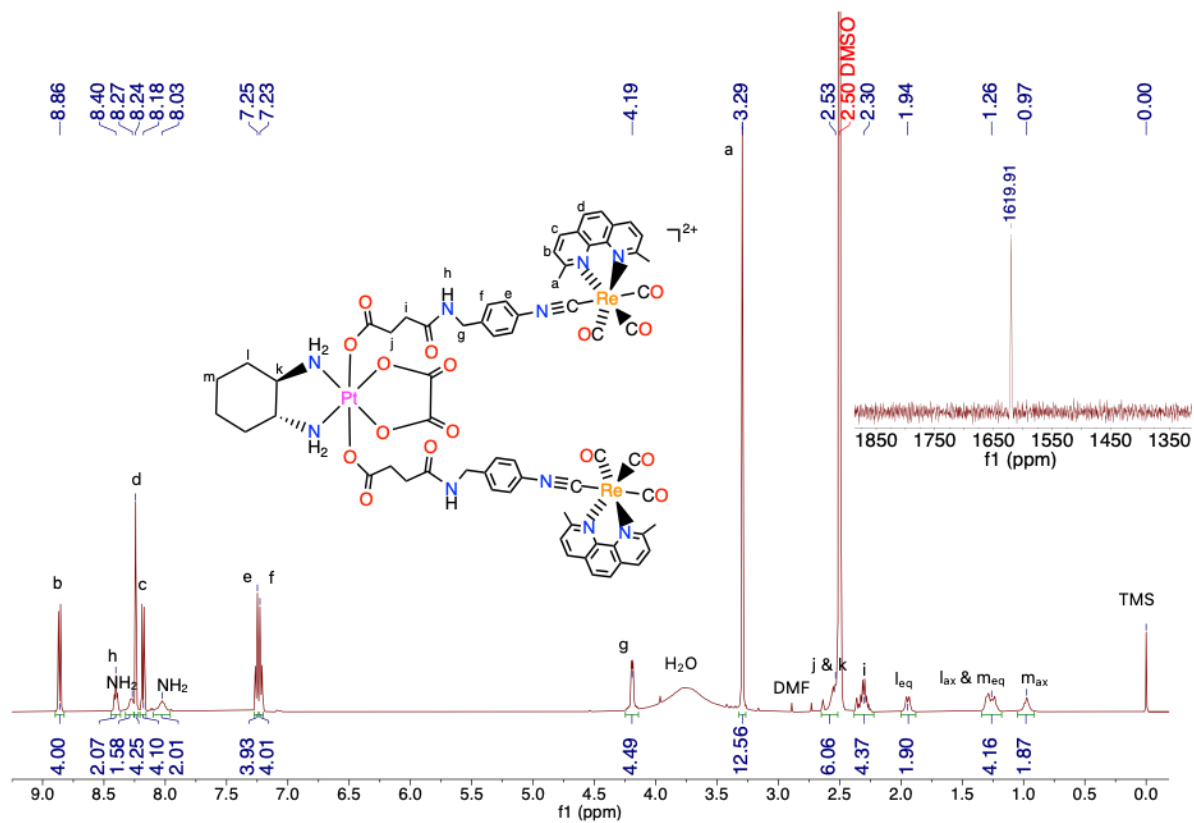


Fig. S3 ^1H NMR spectrum of **OxaliPtRe** in DMSO- d_6 (500 MHz, 25 °C). Inset: ^{195}Pt NMR spectrum of **OxaliPtRe** in DMSO- d_6 (108 MHz, 25 °C).

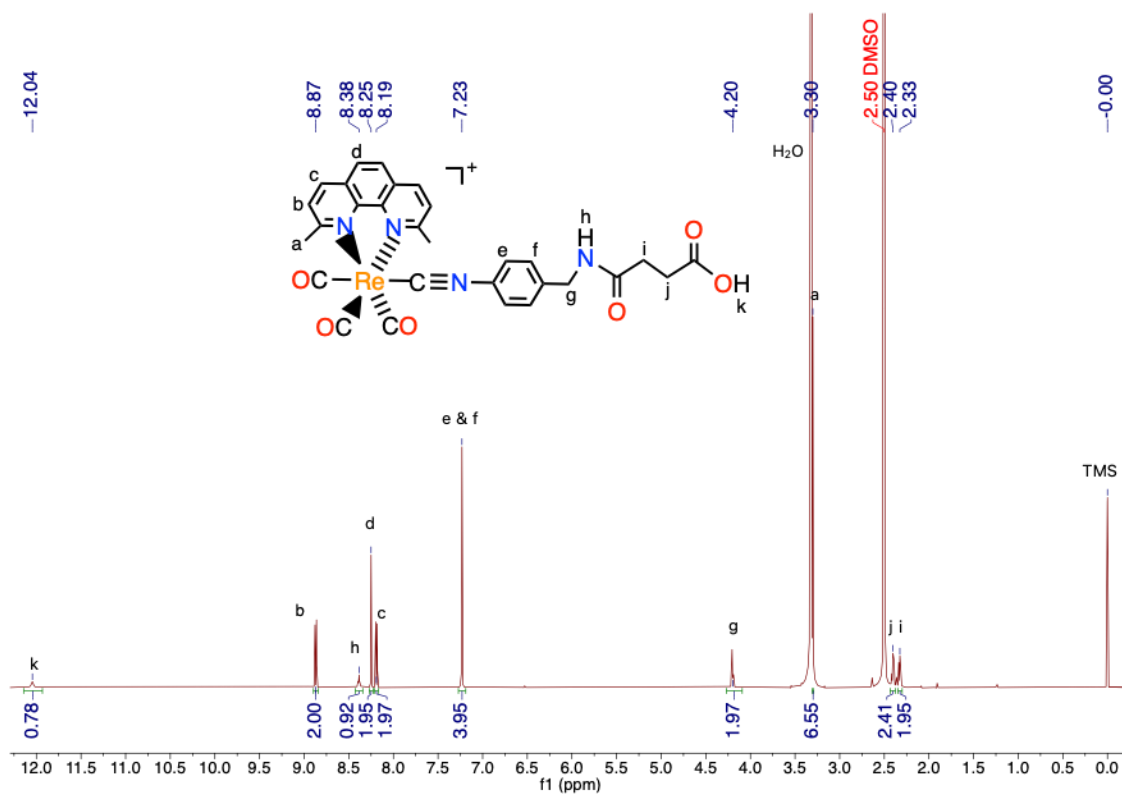


Fig. S4 ^1H NMR spectrum of **TRIP-suc** in DMSO- d_6 (500 MHz, 25 °C).

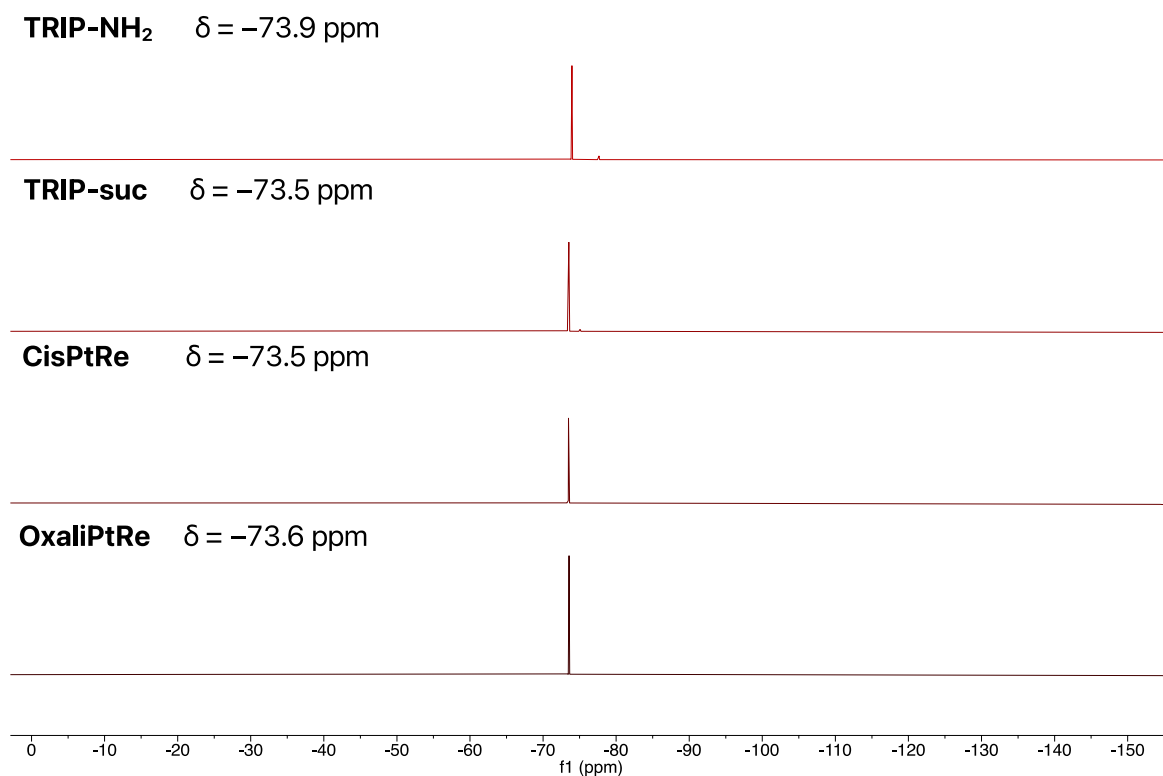


Fig. S5 ^{19}F NMR spectra of **TRIP-NH₂**, **TRIP-suc**, **CisPtRe** and **OxaliPtRe** in DMSO- d_6 (470 MHz, 25 °C).

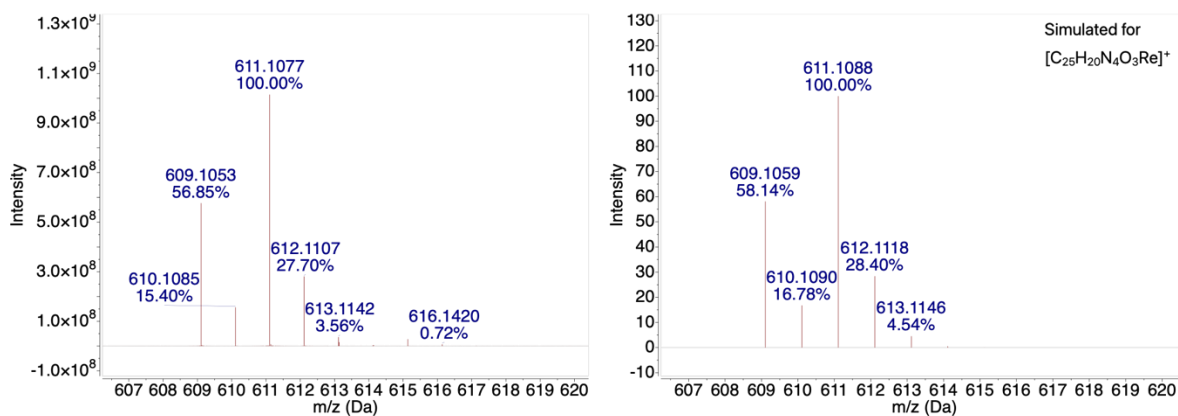


Fig. S6 Experimental (left) and simulated (right) ESI-MS of **TRIP-NH₂**.

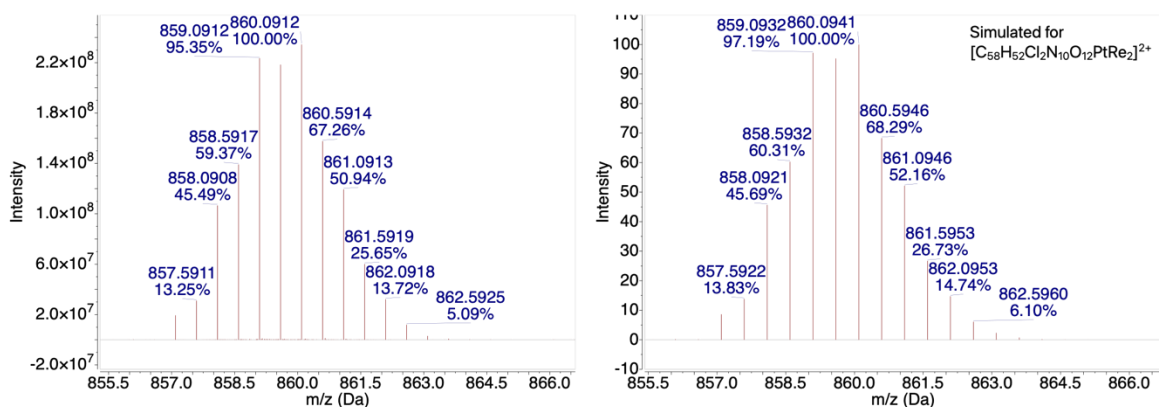


Fig. S7 Experimental (left) and simulated (right) ESI-MS of **CisPtRe**.

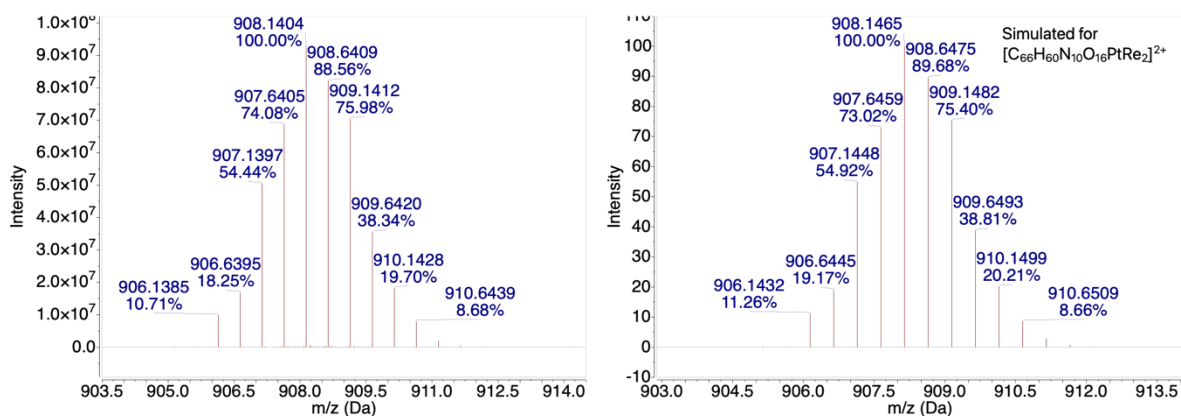


Fig. S8 Experimental (left) and simulated (right) ESI-MS of **OxaliPtRe**.

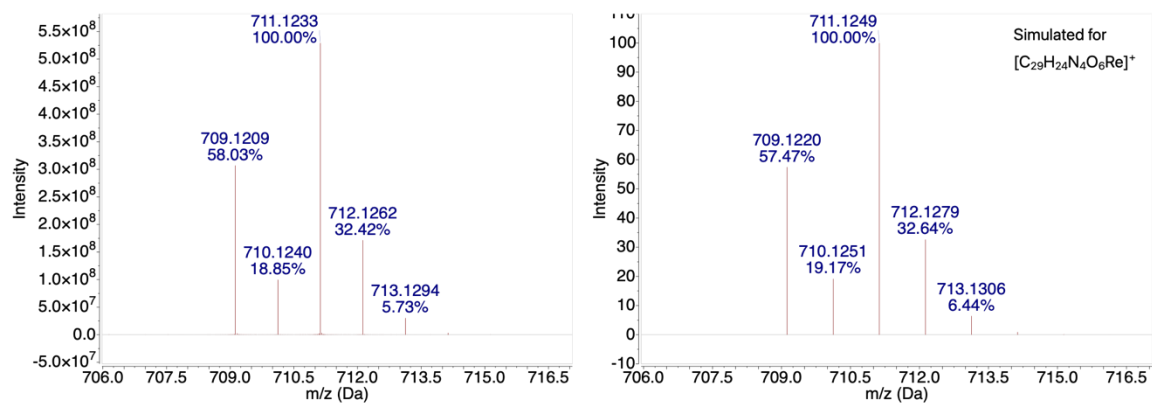


Fig. S9 Experimental (left) and simulated (right) ESI-MS of **TRIP-suc**.

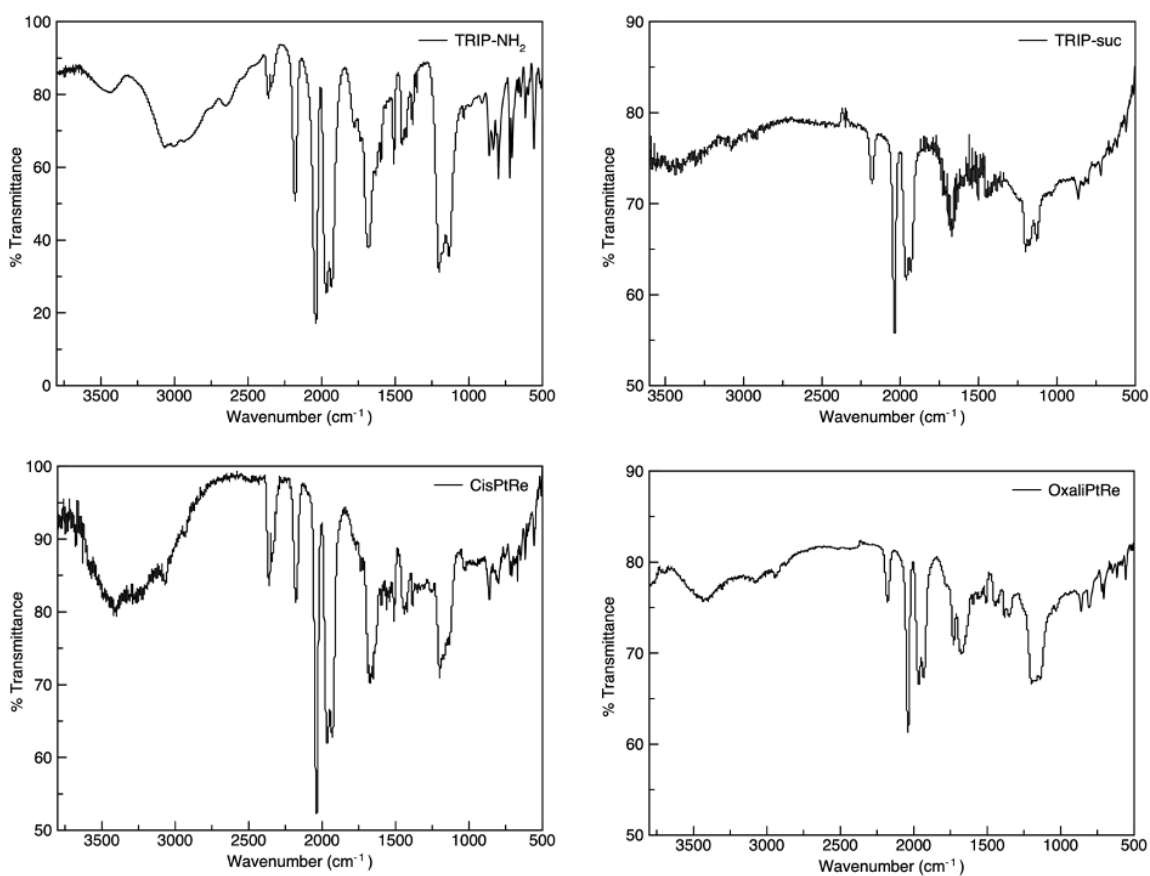


Fig. S10 IR spectra of **TRIP-NH₂**, **TRIP-suc**, **CisPtRe** and **OxaliPtRe**.

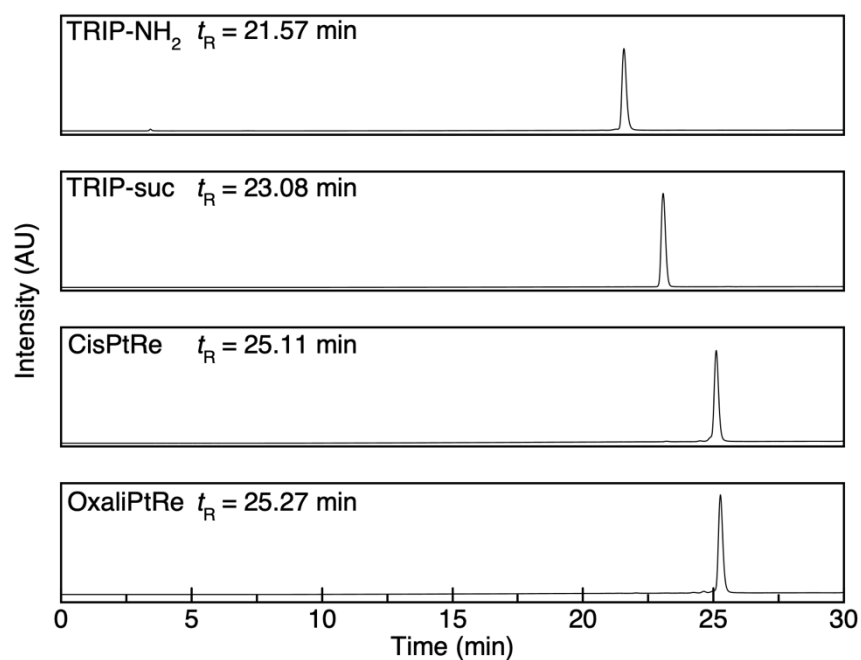


Fig. S11 HPLC chromatograms of **TRIP-NH₂**, **TRIP-suc**, **CisPtRe** and **OxaliPtRe**.

3. Stability and Decomposition Studies

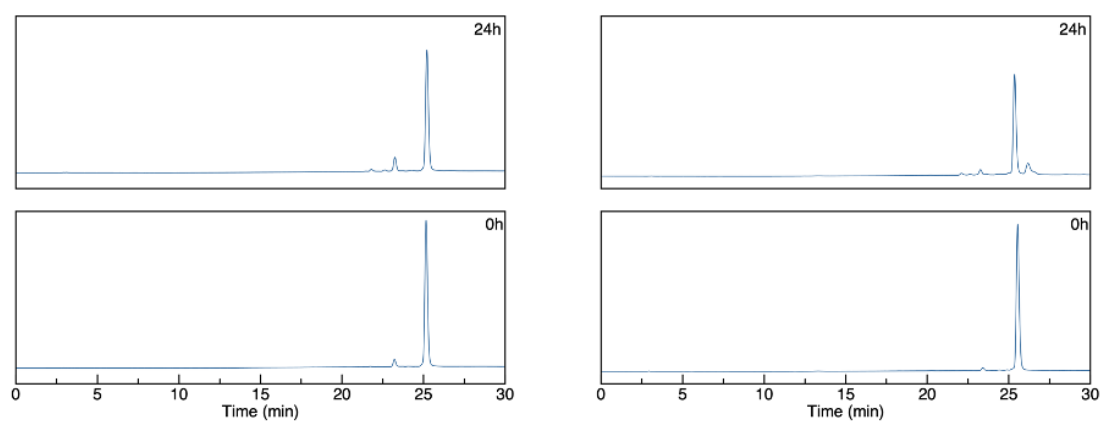


Fig. S12 HPLC chromatograms of 300 μ M **CisPtRe** (left) and **OxaliPtRe** (right) in 20:80 MeOH:PBS at 37 °C from 0 to 24 h.

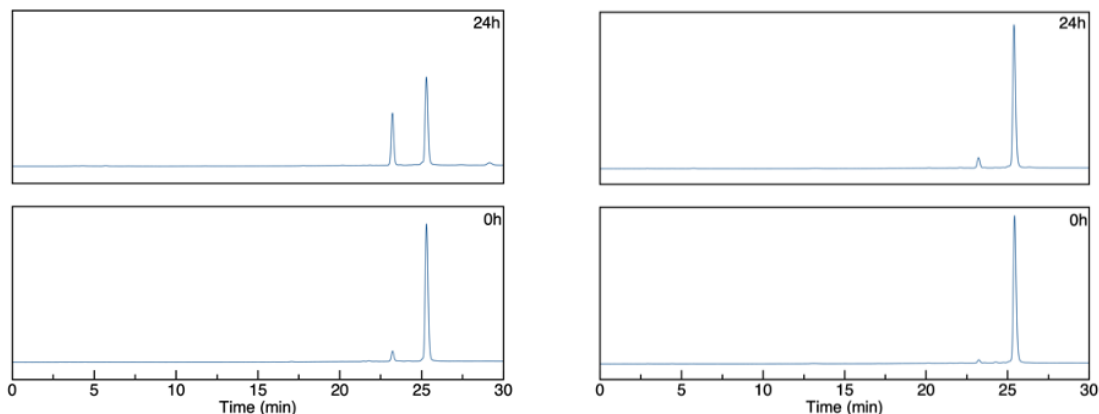


Fig. S13 HPLC chromatograms of 250 μM **CisPtRe** (left) and **OxaliPtRe** (right) in the presence of glutathione (5 mM) in 20:80 MeOH:PBS at 37 °C from 0 to 24 h.

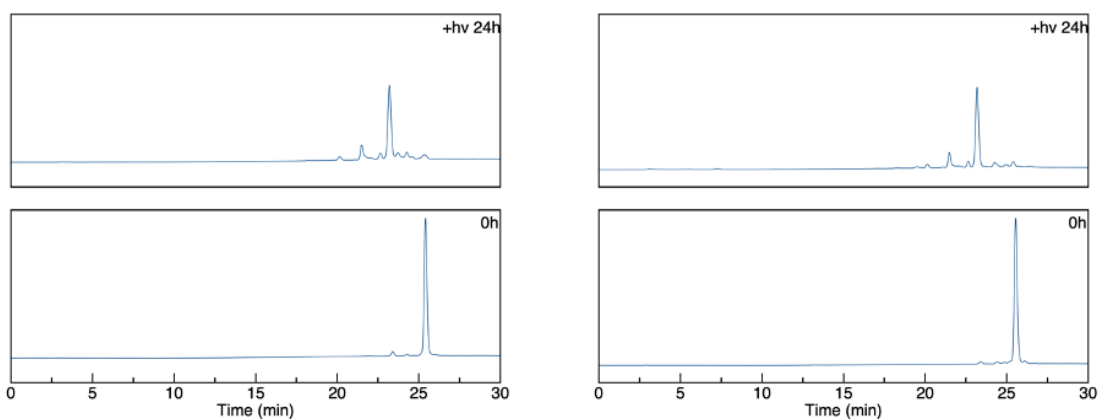


Fig. S14 HPLC chromatograms of 200 μM **CisPtRe** (left) and **OxaliPtRe** (right) in the in 50:50 MeOH:PBS irradiated at 365 nm for 24 h at 37 °C.

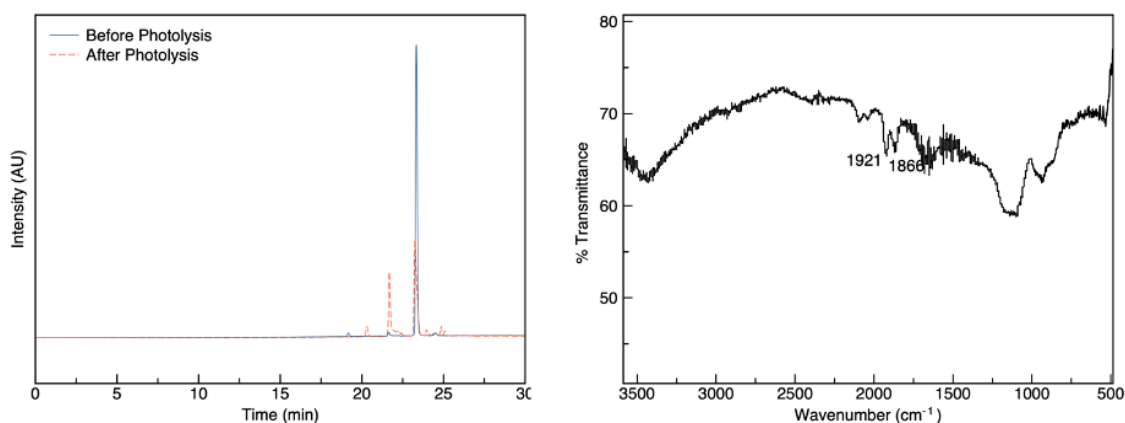


Fig. S15 Left: HPLC chromatograms of 400 μM **TRIP-suc** in 50:50 MeOH:PBS solution before photolysis (blue trace) and after 72 h photolysis (red trace). Right: IR spectrum of the lyophilized photoproducts with the energies of the CO stretches indicated.

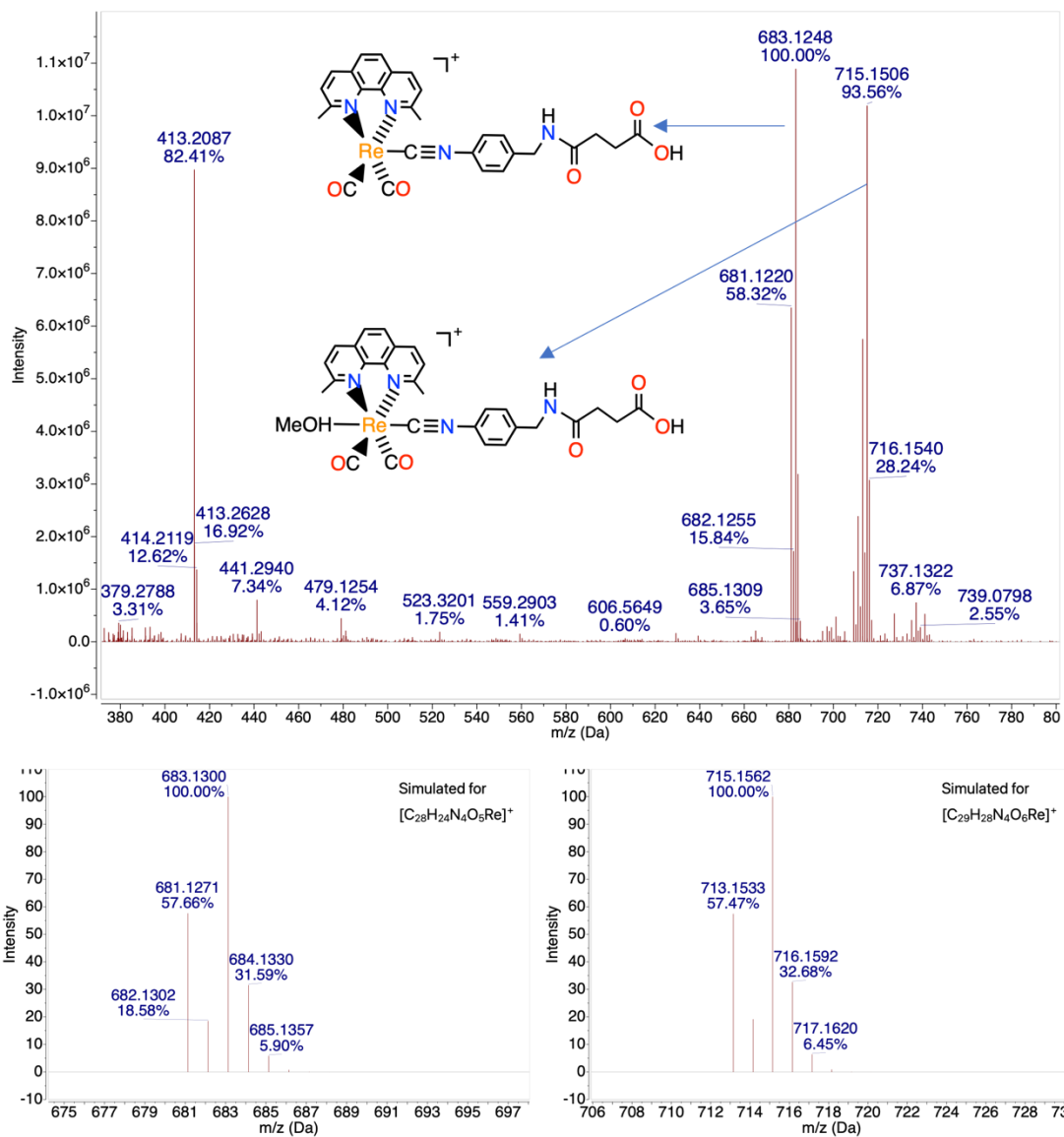


Fig. S16 Top: ESI-MS of **TRIP-suc** upon 72 h photolysis. Bottom: Simulated ESI-MS of the photoproducts.

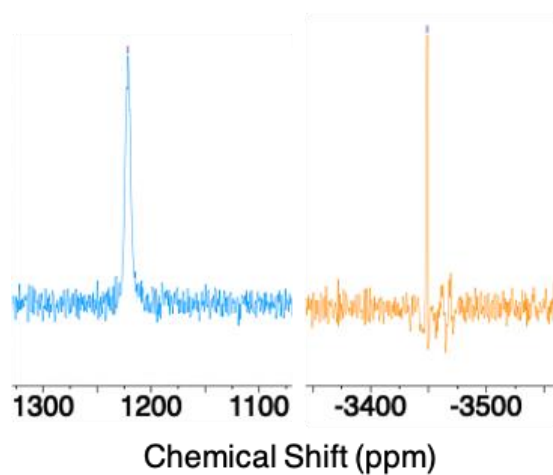


Fig. S17 ^{195}Pt NMR spectra of CisPtRe before (left, blue trace) and after 60 h of photolysis (right, orange trace) in $\text{DMSO-}d_6$ (10 mM) at 25 °C.

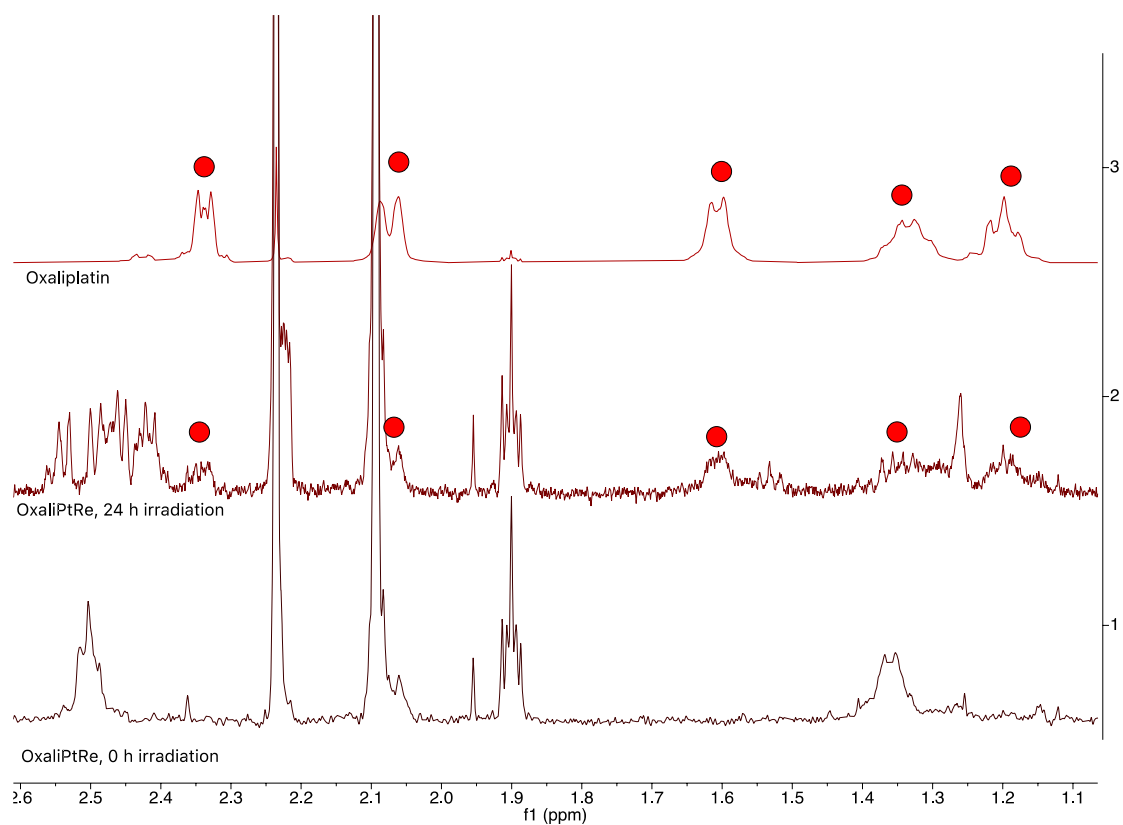


Fig. S18 Aliphatic region of the NMR spectra of 200 μM OxaliPtRe before (bottom trace) and after 24 h of photolysis (middle trace), and oxaliplatin (top trace) in MeOD:Deuterated PBS 50:50 at 25°C. The red circles represent the resonances assignable to the DACH protons of oxaliplatin.

4. Photophysical and Photochemical Studies

Photoluminescence Quantum Yield. Photoluminescence quantum yields were measured relative to the standard quinine sulfate ($\Phi = 0.52$) in 0.05 M H₂SO₄.⁶ The samples were prepared as solutions in PBS with the absorbance below 0.1 to prevent inner filter effects. An excitation wavelength of 350 nm was used for the samples and standards. The absorbance at 350 nm was plotted versus the integrated emission intensity. The slopes (S) of the resulting lines and the refractive index (n) of the solvents were used in the equation to obtain the quantum yields of the samples.

$$\Phi_{\text{sample}} = \Phi_{\text{ref}} (S_{\text{sample}}/S_{\text{ref}}) (n_{\text{sample}}/n_{\text{ref}})^2 \quad (1)$$

Photoluminescence Lifetime. Laser excitation for the phosphorescence lifetime measurements was provided by pulsing the 405 nm laser line from a four-line iChrome MLE laser (Toptica Photonics AG, Munich, Germany). The diode laser in the iChrome was triggered by a DG535 Digital Delay/Pulse Generator (Stanford Research, Sunnyvale, CA) at 100 kHz and delivered 100 ns fwhm 405 nm excitation pulses. The 405 nm pulses were fiber-delivered to a sample-filled cuvette, and phosphorescence was collected at 90° through a second fiber for delivery to a Bialkali photomultiplier tube (HC125, Hamamatsu, Bridgewater, NJ) through a 470 nm long pass filter (HQ470lp, Chroma Technology, Bellows Falls, VT). The time-resolved photon counts were collected in 40 ns time bins using a SR430 Multichannel scaler (Stanford Research, Sunnyvale, CA). Data was transferred to a PC via the SR430 GPIB bus and fit to the standard exponential decay model. Measurements were collected in PBS solutions at 20 μM. For deoxygenated measurements, nitrogen gas was bubbled into the PBS solutions for 15 min, and then the lifetime was determined.

Photochemical Reaction Quantum Yield. The photon flux of the mercury/xenon arc lamp was determined via ferrioxalate actinometry.⁷ Subsequently, all samples were irradiated in 50:50 MeOH:PBS solution with monochromatic 365 nm light at 25 °C for a given time period. The number of photons absorbed was plotted versus the number of molecules formed during this period. The slopes of the resulting lines were the photochemical quantum yields of the samples.⁷ For **TRIP-suc**, the formation of photoproducts was monitored by the UV-vis absorbance change at 449 nm, where the extinction coefficients of the both the starting material and photoproduct had been determined. For **CisPtRe** and **OxaliPtRe**, the reaction progress was monitored by HPLC instead of the UV-Vis, because HPLC can deconvolute the primary photolysis of the **PtRe** from the secondary photolysis of **TRIP-suc**, by the virtue of the difference in retention time between the photoproducts in these two processes. The decomposition of the **PtRe** was monitored by the change in the corresponding chromatogram peak area. To avoid complications in interpretation that may originate from the secondary photolysis, quantum yields were quantified within the first 20% of the reaction progress.

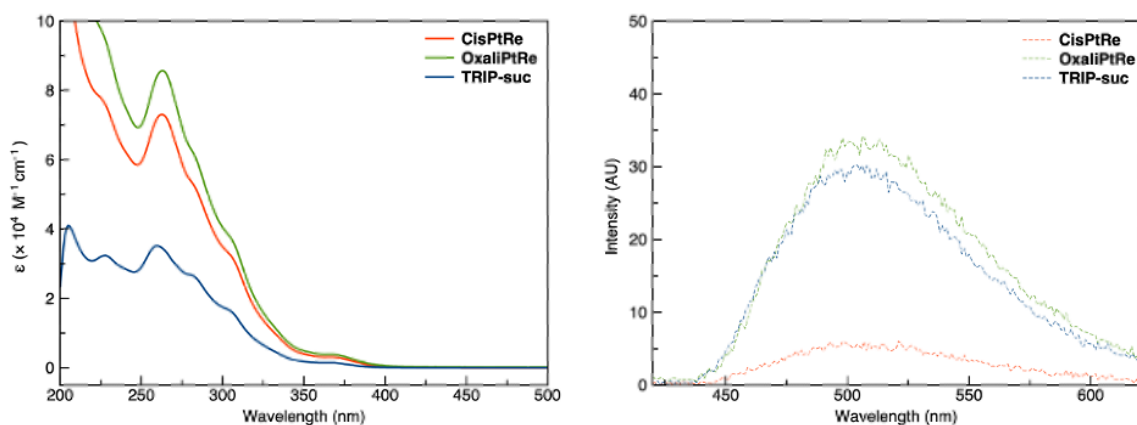


Fig. S19 UV-Vis spectra (left) and emission spectra (right) in pH 7.4 PBS solutions for **CisPtRe**, **OxaliPtRe** and **TRIP-suc** (18 μM) at 25 $^{\circ}\text{C}$.

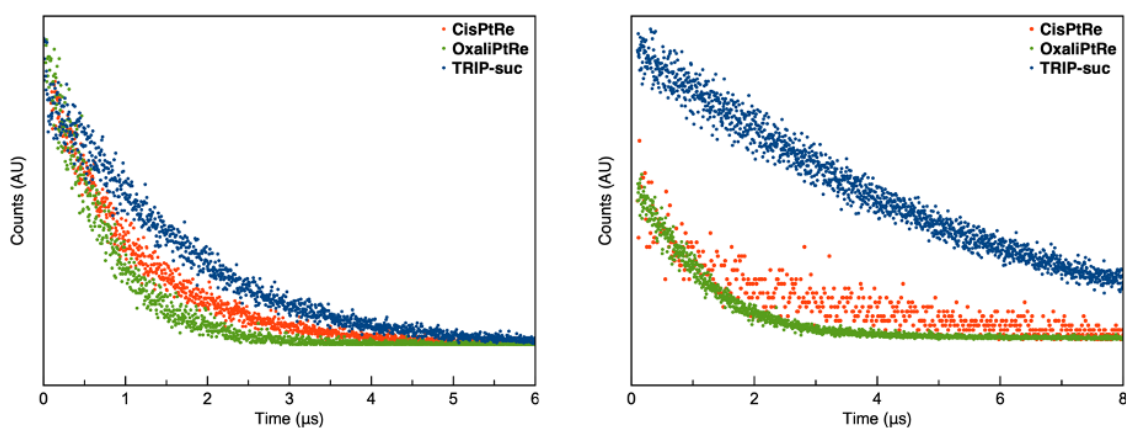


Fig. S20 Transient emission decay profile of **CisPtRe**, **OxaliPtRe** and **TRIP-suc** (20 μM) in pH 7.4 PBS at 25 $^{\circ}\text{C}$ in air-equilibrated solution (left) and under nitrogen (right).

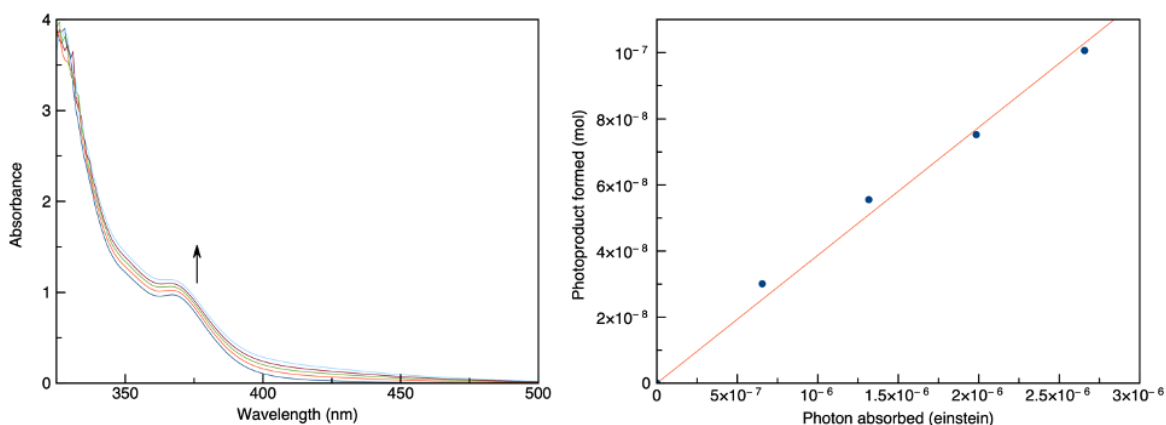


Fig. S21 Left: evolution of the UV-Vis spectrum of **TRIP-suc** (400 μM) in 50:50 MeOH:PBS as it is irradiated at 365 nm over a 20 min period at 25 $^{\circ}\text{C}$. Right: plot of quantity of photoproduct formed versus amounts of photons absorbed.

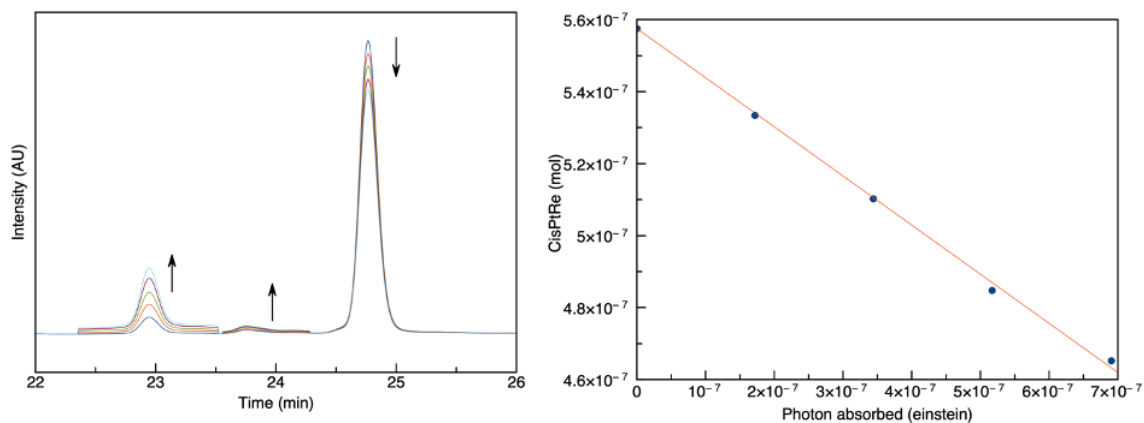


Fig. S22 Left: evolution of the HPLC chromatogram of **CisPtRe** (220 μM) in 50:50 MeOH:PBS as it is irradiated at 365 nm over a 4 min period at 25 $^{\circ}\text{C}$. Right: plot of quantity of starting material decomposed versus amounts of photons absorbed.

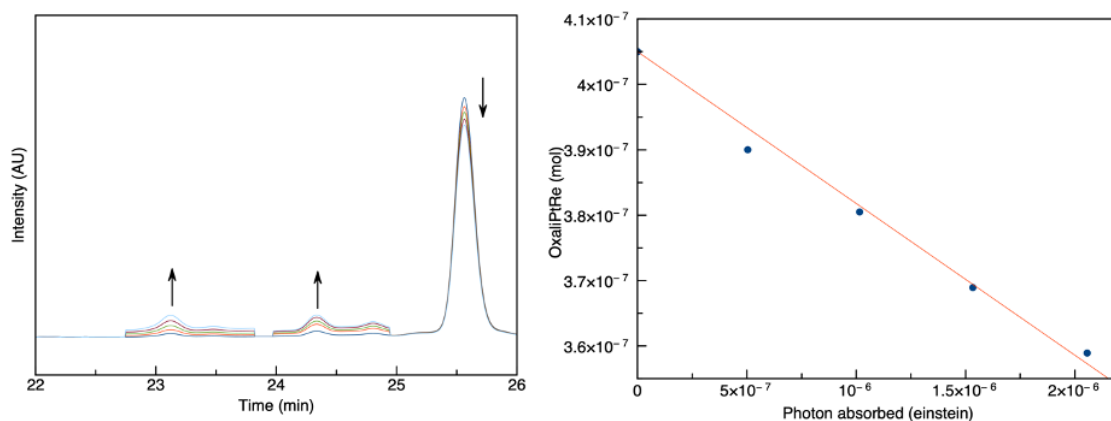


Fig. S23 Left: evolution of the HPLC chromatogram of **OxaliPtRe** (160 μM) in 50:50 MeOH:PBS as it is irradiated at 365 nm over a 20 min period at 25 $^{\circ}\text{C}$. Right: plot of quantity of starting material decomposed versus amounts of photons absorbed.

5. Electrochemical Studies

Cyclic Voltammetry: Electrochemical measurements were carried out using a Pine WaveNow potentiostat with a three-electrode setup consisting of a glassy carbon working electrode, a platinum counter electrode, and a Ag wire quasi-reference electrode. Complexes were dissolved in anhydrous DMF with 0.10 M [Bu₄N][PF₆] (TBAP) as the supporting electrolyte. Potentials were referenced using an internal standard of the ferrocene/ferricenium couple at 0.45 V.

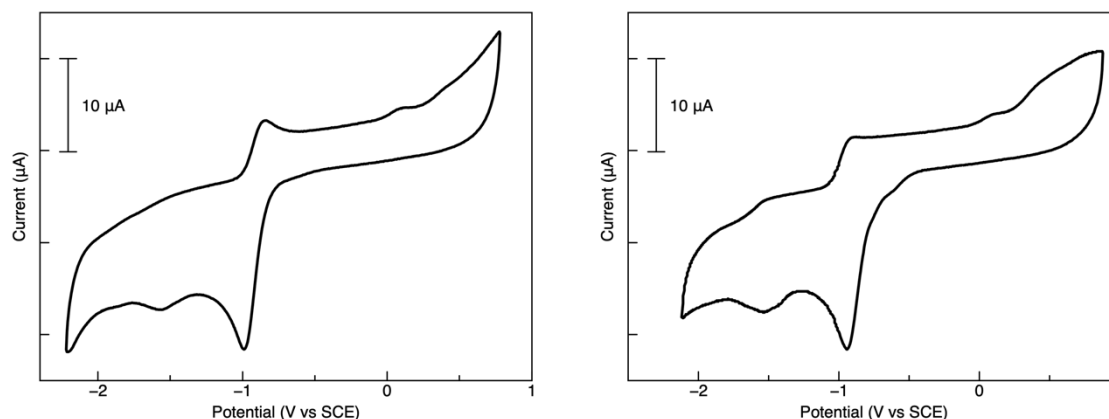


Fig. S24 Cyclic voltammograms of **CisPtRe** (left) and **OxaliPtRe** (right) in DMF with 0.1 M TBAP at 25°C and 0.1 V/s scan rate.

5. Computational Studies

DFT calculations were performed using Gaussian 16.⁸ Geometry optimizations were performed in the gas phase using the BP86 functional⁹ without symmetry restraints. The LANL2DZ basis set and effective core potential¹⁰ were utilized for both rhenium and platinum atoms, and the 6-31G(d,p) basis set^{11,12} was used for the other elements. After geometry optimization, frequency calculations were carried out to ensure that the geometries had converged to local minima on the potential energy surface. The Cartesian coordinates of all optimized structures are provided as part of the Electronic Supplemental Information. Using these optimized geometries, subsequent molecular orbital and time-dependent DFT (TD-DFT) calculations were performed using the hybrid B3LYP functional^{13,14} and a polarizable continuum model (PCM)¹⁵ to simulate solvation of the compounds in water. Through TD-DFT, 20 lowest triplet excited states were calculated for **TRIP-suc** and 50 lowest triplet excited states were calculated for **CisPtRe** and **OxaliPtRe**. Relevant excited states were subjected to natural transition orbitals (NTOs) analysis, which transforms multiple transitions in a specific excited state into a single pair of orbitals, giving a simplified picture of the excited states.¹⁶ The isodensity surface plots of the FMOs and NTOs are rendered at an isovalue of 0.02 using Avogadro 1.2.0.¹⁷

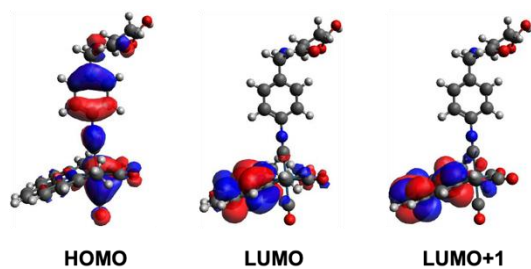


Fig. S25 Frontier Kohn-Sham molecular orbitals of **TRIP-suc**.

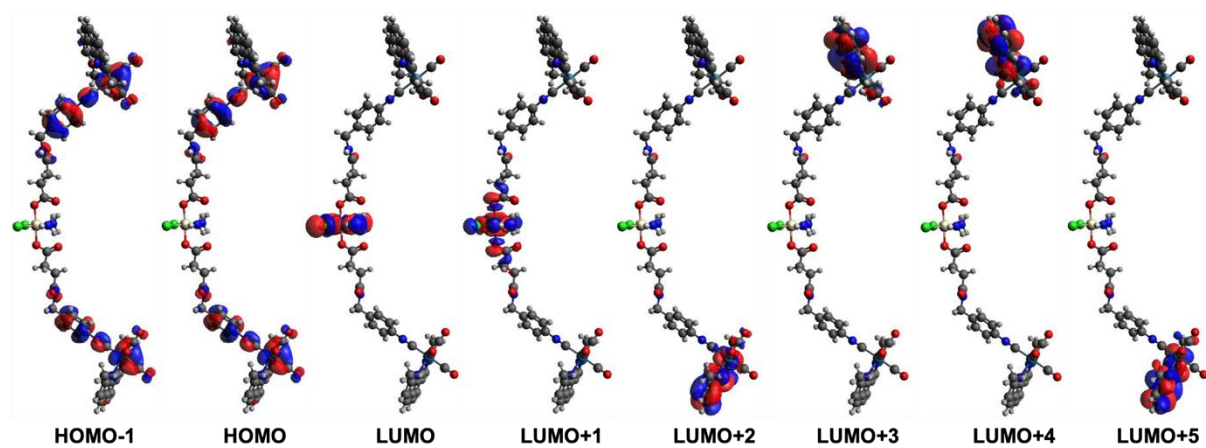


Fig. S26 Frontier Kohn-Sham molecular orbitals of **CisPtRe**.

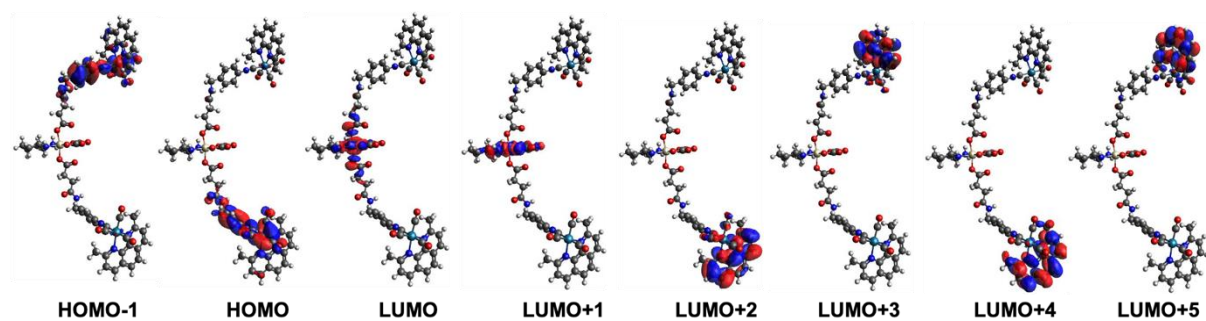


Fig. S27 Frontier Kohn-Sham molecular orbitals of **OxaliPtRe**.

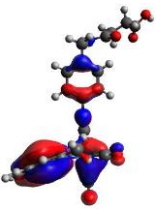
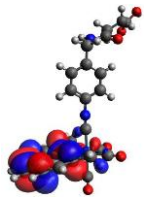
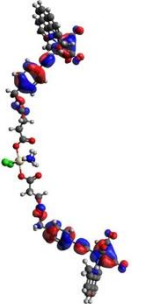
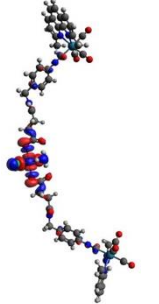
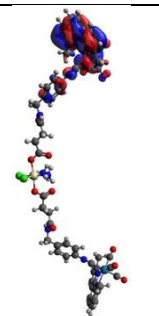
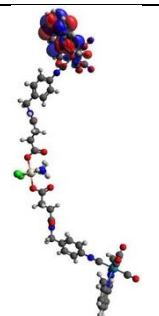
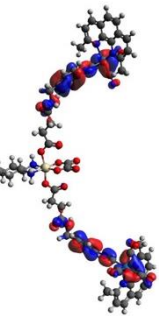
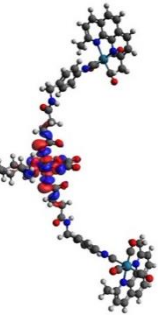
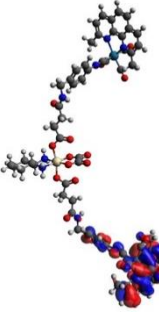
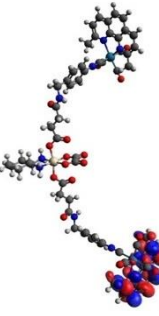
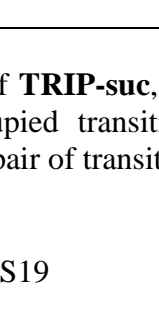
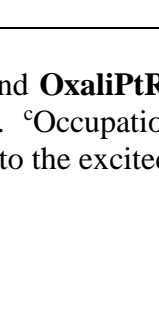
Complex	Excited State	HOTO ^a	LUTO ^b
TRIP-suc	T ₆ E = 3.64 eV w ^c = 0.85 ³ MLCT/ ³ ILCT/ ³ LLCT		
	T ₁₁ E = 3.05 eV w = 0.90 ³ MMCT		
CisPtRe	T ₄₄ E = 3.65 eV w = 0.81 ³ MLCT/ ³ ILCT/ ³ LLCT		
	T ₁₆ E = 3.45 eV w = 0.99 ³ MMCT		
OxaliPtRe	T ₂₃ E = 3.65 eV w = 0.84 ³ MLCT/ ³ ILCT/ ³ LLCT		
	T ₁₆ E = 3.45 eV w = 0.99 ³ MMCT		

Fig. S28 NTOs for relevant excited states of **TRIP-suc**, **CisPtRe**, and **OxaliPtRe**. ^aHighest occupied transition orbitals. ^bLowest occupied transition orbitals. ^cOccupation numbers representing the contribution of the specific pair of transition orbitals to the excited state.

6. Cellular Studies

Cell Lines and Culture Conditions. The HeLa (cervical cancer) cell line was obtained from American Type Culture Collection (ATCC) and cultured using Dulbecco's Modified Eagle's Medium (DMEM) supplemented with 10% fetal bovine serum (FBS). A2780 (ovarian cancer) and A2780CP70 (cisplatin-resistant ovarian cancer) cell lines were provided by the Cell Culture Facility of Fox Chase Cancer Center (Philadelphia, PA, USA). These cells were cultured as monolayers with Roswell Park Memorial Institute (RPMI)-1640 culture media supplemented with 10% FBS. All cell lines were grown in a humidified incubator at 37 °C with an atmosphere of 5% CO₂. Cells were passed at 80–90% confluence using trypsin/EDTA. Cells were tested for mycoplasma contamination bimonthly through the commercial service provided by the College of Veterinary Medicine at Cornell University.

Cytotoxicity Assay. The procedure for determining phototoxicity was modified from the OECD Guidelines, except 3-(4,5-dimethylthiazol-2-yl)-2,5-tetrazolium bromide (MTT) was used instead of Neutral Red to determine cell viability.¹⁸ A2780 or A2780CP70 cells were seeded in 96-well plates with 4000 cells/well in 100 μ L of growth media and allowed to reattach overnight. The following day, the culture media was removed and replaced with 200 μ L of media containing varying concentration of the complexes. The cells were incubated for 3 h and then irradiated with 365 nm light for 1 h (one plate under the same dosing conditions was kept outside the incubator in the dark as a control). The light source was a UVA handlamp elevated 8 cm from the cells to give a photon flux of $(2.38 \pm 0.31) \times 10^{-10}$ einstein/s. After exposure to light, the plates were incubated for an additional 44 h, the medium was removed from the wells, and MTT in RPMI (200 μ L, 1 mg/mL) was added. The additional 44 h incubation was performed to ensure that the cells were in the logarithmic growth phase and that the cells had adequate time to regrow after exposure to the complexes. After 4 h, the media was removed, and the purple formazan crystals were dissolved in 200 μ L of an 8:1 mixture of DMSO and pH 10 glycine buffer. The absorbance at 570 nm in each well was measured using a BioTek Synergy HT plate reader. Cell viability was determined by normalizing the absorbance of the treated wells to untreated wells. Results are reported as the average cell viability of six replicates per concentration from three independent trials.

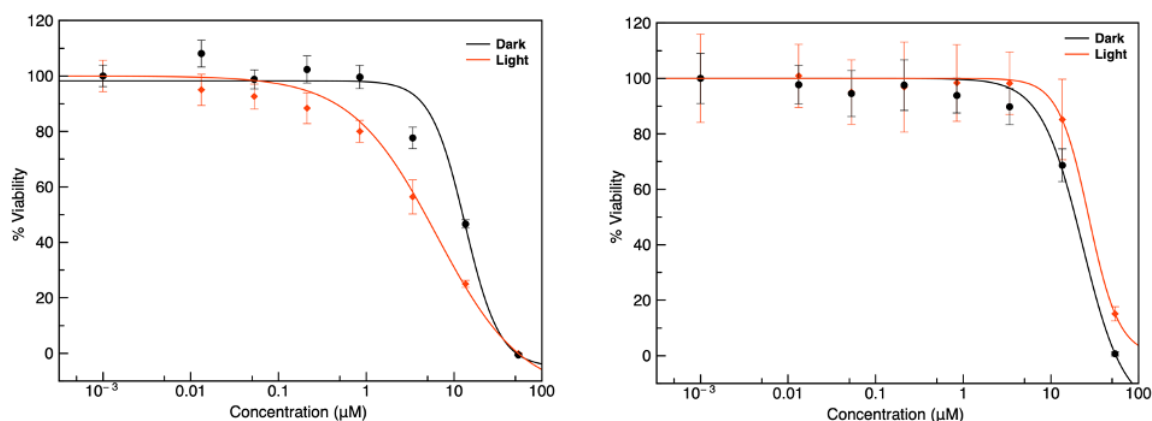


Fig. S29 Dose-response curve of **CisPtRe** under dark (black) and 365 nm light (red) conditions in A2780 (left) and A2780CP70 (right) cells.

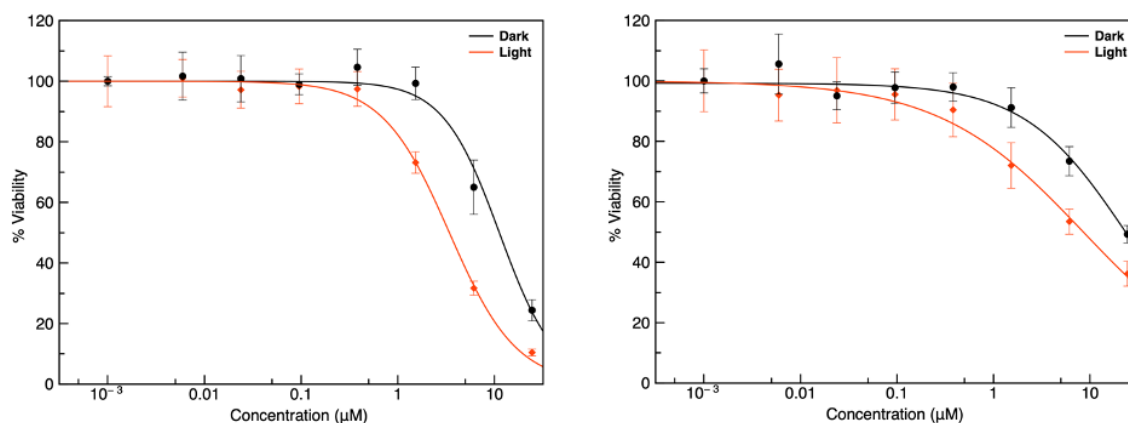


Fig. S30 Dose-response curve of **OxaliPtRe** under dark (black) and 365 nm light (red) conditions in A2780 (left) and A2780CP70 (right) cells.

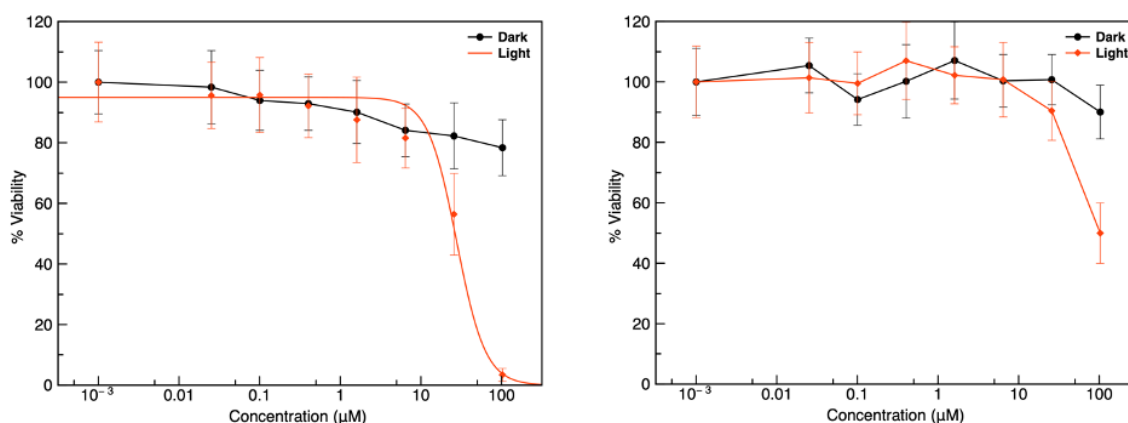


Fig. S31 Dose-response curve of **TRIP-suc** under dark (black) and 365 nm light (red) conditions in A2780 (left) and A2780CP70 (right) cells.

7. XRF Imaging Studies

Sample Preparation. HeLa cells were plated on 1.5 mm × 1.5 mm × 500 nm silicon nitride windows (Norcada, Canada) attached to 100 mm × 20 mm tissue culture dishes and allowed to grow to 70–80% confluency. The culture media was replaced with 6 mL of 8.5 μM **OxaliPtRe** in media and the cells were incubated for 3 h at 37 °C. Control cells were prepared following an identical procedure but without addition of **OxaliPtRe**. Following the incubation, one dish of cells was irradiated with 365 nm light for 1 h using the aforementioned UVA handlamp, and the other dish under the same condition was kept outside the incubator in the dark as a control. After exposure to light, the dishes were incubated for additional 3 h. The cells were washed with PBS (2 × 6 mL) and fixed using 6 mL of 4% paraformaldehyde in PBS for 15 minutes. Following fixation, cells were rinsed with 2 × 6 mL of an aqueous ammonium acetate solution (100 mM) and 2 × 6 mL of MilliQ water. The windows were dried using lens paper and stored over drying agent (Drierite™) until analysis.

Data Collection. XRF imaging yielding elemental distribution maps of single treated cells was conducted at beamline 2-ID-D at the Advanced Photon Source at Argonne National Laboratory.

This beamline uses double multilayer monochromator and a gold “high flux” zone plate setup to focus the monochromatic beam into a spot of ~300-400 nm FWHM in diameter. A single element Si drift energy dispersive detector (Vortex EX, SII nanotechnology, Northridge, CA) at 90° to the incident beam was used to collect the fluorescence signal from the samples. All measurements were performed under a helium atmosphere. Individual cells treated under the conditions described above were selected at the beamline by inspection with an optical microscope before mounting and irradiating the sample. An incident beam energy of 14.0 keV was used to excite K-edge fluorescence from the biologically relevant non-metal (P, S, Cl) and first row transition metal (Fe, Cu, Zn, etc.) elements. The incident beam energy was also sufficient to achieve L-edge fluorescence of Re and Pt and hence map the intracellular distribution and co-localization of these elements. The sample was raster-scanned with a step-size of 0.5 μm and a beam dwell time of 1000 ms per spatial point.

Data Analysis. The analysis of the XRF elemental maps was performed using the MAPS software package. The fluorescence spectrum of each spatial point from the samples was fit to a sum of Gaussian functions, modified by the addition of a step function and a tailing function to describe incomplete charge collection and detector artefacts. Quantification was performed by comparison to the corresponding measurements on the thin film standards NBS-1832 and NBS-1833 from the Nation Bureau of Standards (Gaithersburg, MD). The integrated fluorescence spectra extracted from the regions of interest corresponding to individual cells were fit by a sum of modified Gaussian functions to determine average elemental area densities (units of $\mu\text{g cm}^{-2}$).

Supplemental Discussion. Assessment of intracellular elemental contents across several cells within each group by integration of the characteristic X-ray fluorescence signals for a range of endogenous elements (P, S, Ca, Fe, Cu, Zn) found no significant perturbations between untreated and treated cells, nor between the irradiated and non-irradiated cells. The levels of Pt and Re in untreated cells was below the detection limit; significant increases were noted in the cellular content of both metals between the untreated and treated cells (Fig. S35, ESI†).

The apparent ratio of Re:Pt contents in all treated cells was closer to 1:1 than the 2:1 that would be expected if the conjugate was taken up intact and no efflux favoring one metal over the other had occurred. However, we cannot confidently distinguish between these two ratios, because a significant background of Pt L fluorescence was detected in the control cell images and in the regions of the treated cell images outside of the cell area. This background was attributed to secondary fluorescence from an upstream order sorting aperture constructed of Pt metal, and distribution of the signal in the control samples was spatially invariant and not consistent with the cell structure. The magnitude of this background signal was estimated by fitting to the spatially integrated spectrum from the non-cell region of the control sample cells, and that background was then subtracted from the whole-cell quantitation shown in Figure S35. As such, Figure S35 shows no bar for the control sample as the background subtraction sets the value to a value below the estimated detection limit for Pt in these samples.

A statistically significant decrease of between two and three-fold was observed in the average intracellular contents of both Pt and Re in irradiated treated cells compared to cells that were not irradiated (Fig. S35, ESI†). This observation suggests that irradiation stimulates an as yet unknown efflux mechanism for the conjugate, or its decomposition products, but this interpretation warrants investigation by an alternative method, such as ICP-MS, which is capable of measuring post-treatment concentrations of the metals in media as well as in cells.

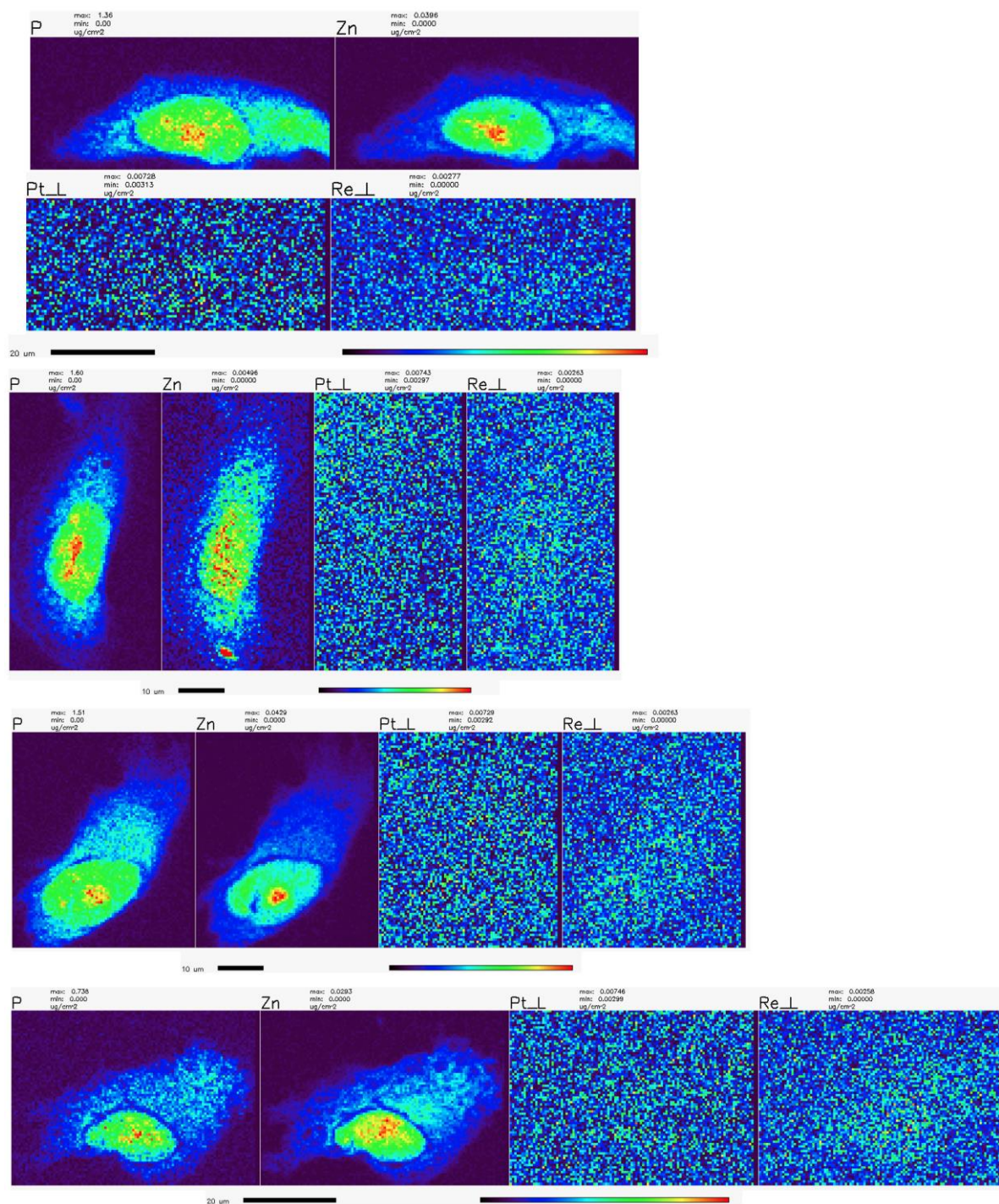


Fig. S32 X-ray fluorescence elemental distribution maps (P, Zn, Pt and Re) of untreated HeLa cells fixed to silicon nitride windows. The maximal elemental area density (units of $\mu\text{g}/\text{cm}^2$) is given in each map. An “L” denotes that the fluorescence map was measured using the L fluorescence lines of this element. XRF elemental maps were collected using an incident beam energy of 14.0 keV, a step-size of 0.5 μm and a dwell time of 1000 ms.

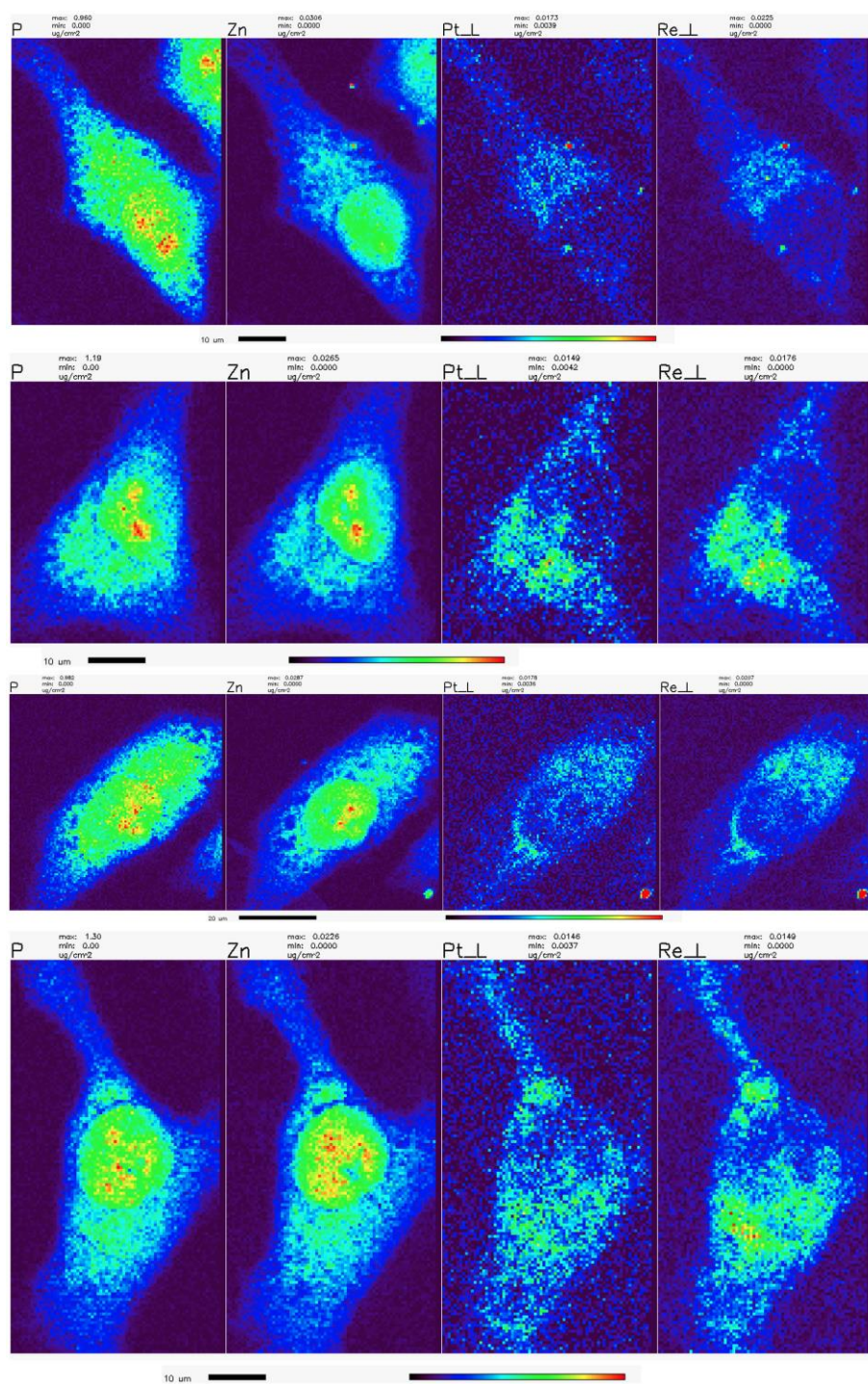


Fig. S33 X-ray fluorescence elemental distribution maps (P, Zn, Pt and Re) of HeLa cells treated with 8.5 μM **OxaliPtRe** in media in the dark for 7 h and then fixed to silicon nitride windows. The maximal elemental area density (units of $\mu\text{g cm}^{-2}$) is given in each map. An “L” denotes that the fluorescence map was measured using the L fluorescence lines of this element. XRF elemental maps were collected using an incident beam energy of 14.0 keV, a step-size of 0.5 μm and a dwell time of 1000 ms.

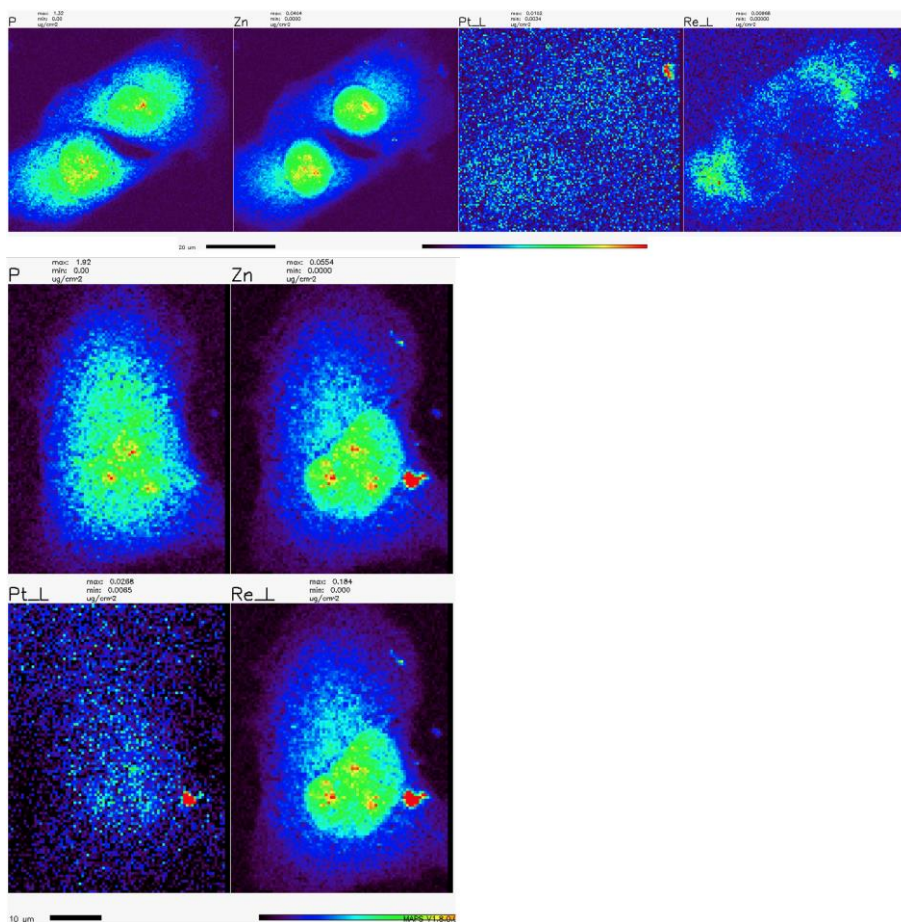


Fig. S34 X-ray fluorescence elemental distribution maps (P, Zn, Pt and Re) of HeLa cells treated with 8.5 μM **OxaliPtRe** in media for 7 h including irradiation at 365 nm for 1 h, starting 3 h into the treatment, and then fixed to silicon nitride windows. The maximal elemental area density (units of μg cm⁻²) is given in each map. An “L” denotes that the fluorescence map was measured using the L fluorescence lines of this element. XRF elemental maps were collected using an incident beam energy of 14.0 keV, a step-size of 0.5 μm and a dwell time of 1000 ms.

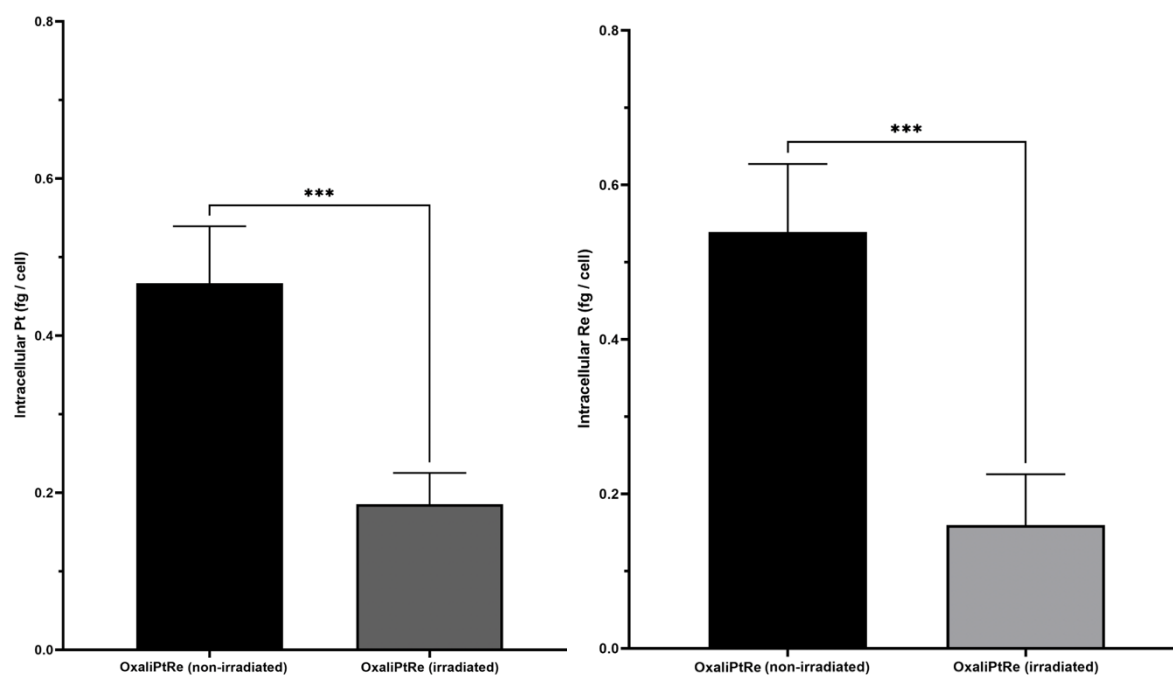


Fig. S35 Average intracellular Pt (left) and Re (right) contents of HeLa cells treated with either **OxaliPtRe** that had been kept non-irradiated or **OxaliPtRe** that was exposed to irradiation of 365 nm light for 1 hour. Per-pixel spectrum fitting and elemental quantitation of the raw XRF data were performed using the MAPS software package. Error bars represent mean \pm SD. *** $p < 0.0002$, Student's unpaired t-test. Background Pt fluorescence was estimated by drawing ROIs around non-cell parts of the image and fitting and quantifying the Pt fluorescence from these ROIs. From these results, a baseline subtraction of 0.81 fg/cell was applied uniformly to all calculations of intracellular Pt content.

8. References

- 1 J. M. Smieja and C. P. Kubiak, *Inorg. Chem.*, 2010, **49**, 9283–9289.
- 2 M. R. Reithofer, S. M. Valiahd, M. A. Jakupec, V. B. Arion, A. Egger, M. Galanski and B. K. Keppler, *J. Med. Chem.*, 2007, **50**, 6692–6699.
- 3 M. Jörg, A. Glukhova, A. Abdul-Ridha, E. A. Vecchio, A. T. N. Nguyen, P. M. Sexton, P. J. White, L. T. May, A. Christopoulos and P. J. Scammells, *J. Med. Chem.*, 2016, **59**, 11182–11194.
- 4 G. W. Gokel, R. P. Widera and W. P. Weber, *Org. Synth.*, 1976, **55**, 96.
- 5 R. Gladysz, Y. Adriaenssens, H. De Winter, J. Joossens, A.-M. Lambeir, K. Augustyns and P. Van Der Veken, *J. Med. Chem.*, 2015, **58**, 9238–9257.
- 6 A. M. Brouwer, *Pure Appl. Chem.*, 2011, **83**, 2213–2228.
- 7 M. Montalti, A. Credi, L. Prodi and M. T. Gandolfi, in *Handbook of Photochemistry*, CRC Press, Boca Raton, FL, 3rd edn., 2006, pp. 601–604.
- 8 M. J. Frisch, G. W. Trucks, H. B. Schlegel, G. E. Scuseria, M. A. Robb, J. R. Cheeseman, G. Scalmani, V. Barone, G. A. Petersson, H. Nakatsuji, X. Li, M. Caricato, A. V. Marenich, J. Bloino, B. G. Janesko, R. Gomperts, B. Mennucci, H. P. Hratchian, J. V. Ortiz, A. F. Izmaylov, J. L. Sonnenberg, D. Williams-Young, F. Ding, F. Lipparini, F. Egidi, J. Goings, B. Peng, A. Petrone, T. Henderson, D. Ranasinghe, V. G. Zakrzewski, J. Gao, N. Rega, G. Zheng, W. Liang, M. Hada, M. Ehara, K. Toyota, R. Fukuda, J. Hasegawa, M. Ishida, T. Nakajima, Y. Honda, O. Kitao, H. Nakai, T. Vreven, K. Throssell, J. A. M. Jr., J. E. Peralta, F. Ogliaro, M. J. Bearpark, J. J. Heyd, E. N. Brothers,

- K. N. Kudin, V. N. Staroverov, T. A. Keith, R. Kobayashi, J. Normand, K. Raghavachari, A. P. Rendell, J. C. Burant, S. S. Iyengar, J. Tomasi, M. Cossi, J. M. Millam, M. Klene, C. Adamo, R. Cammi, J. W. Ochterski, R. L. Martin, K. Morokuma, O. Farkas, J. B. Foresman and D. J. Fox, *Gaussian 16, Revision C.01*, Gaussian, Inc., Wallingford, CT, 2016.
- 9 A. D. Becke, *Phys. Rev. A*, 1988, **38**, 3098–3100.
- 10 P. J. Hay and W. R. Wadt, *J. Chem. Phys.*, 1985, **82**, 299–310.
- 11 W. J. Hehre, R. Ditchfield and J. A. Pople, *J. Chem. Phys.*, 1972, **56**, 2257–2261.
- 12 P. C. Hariharan and J. A. Pople, *Theor. Chim. Acta*, 1973, **28**, 213–222.
- 13 C. Lee, W. Yang and R. G. Parr, *Phys. Rev. B*, 1988, **37**, 785–789.
- 14 A. D. Becke, *J. Chem. Phys.*, 1993, **98**, 5648–5652.
- 15 S. Miertuš, E. Scrocco and J. Tomasi, *Chem. Phys.*, 1981, **55**, 117–129.
- 16 R. L. Martin, *J. Chem. Phys.*, 2003, **118**, 4775–4777.
- 17 M. D. Hanwell, D. E. Curtis, D. C. Lonie, T. Vandermeersch, E. Zurek and G. R. Hutchison, *J. Cheminform.*, 2012, **4**, 17.
- 18 OECD Guideline For Testing of Chemicals: In Vitro 3T3 NRU Phototoxicity Test, https://www.oecd-ilibrary.org/environment/test-no-432-in-vitro-3t3-nru-phototoxicity-test_9789264071162-en, (accessed 21 August 2021).